Abstract

Computation in nervous systems depend on the initiation, propagation and inhibition of electrical impulses along the membranes of neurons, leading to synaptic activity connecting neurons. The underlying electrical excitability of cells is possible because the movement of a few charges controls the flow of many charges. This is often mediated by the voltage sensors of voltage gated ion channels. In particular, the S4 voltage sensor of the *Shaker* K^+ ion channel is an experimentally well characterized example presented here in terms of a boundary element method for calculating the electrostatic potential energy and thus predicting expectations of measures.

The path from a theoretical description of the voltage sensor to a prediction of a model's macroscopic consequences requires simulation since such models have not been solved analytically. However, given that this behavior depends on the electrostatic properties of complex three-dimensional dielectric regions that are inhomogeneous, the implementation in simulation must be treated as a scientific instrument with robust controls and sensitivity analysis. By taking this approach, it is possible to build a model that is comparable with biological experiment, can be decomposed for analysis and hypothesis, and can be used as an element in larger scale models of full ion channels.

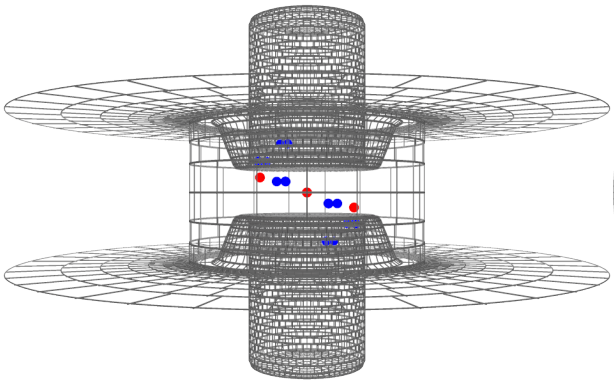

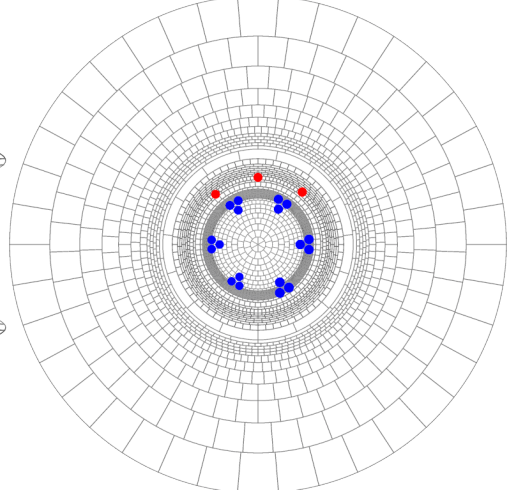

JÜLICH
FORSCHUNGSZENTRUM

Electrostatics of the Voltage Sensor of Ion Channels:

Simulation as a science

24. July, 2014 | Alexander Peyser | Simulation Lab Neuroscience, Forschungszentrum Jülich

Computation

Computation in nervous systems depend on the initiation, propagation and inhibition of electrical impulses along the membranes of neurons, leading to synaptic activity connecting neurons.

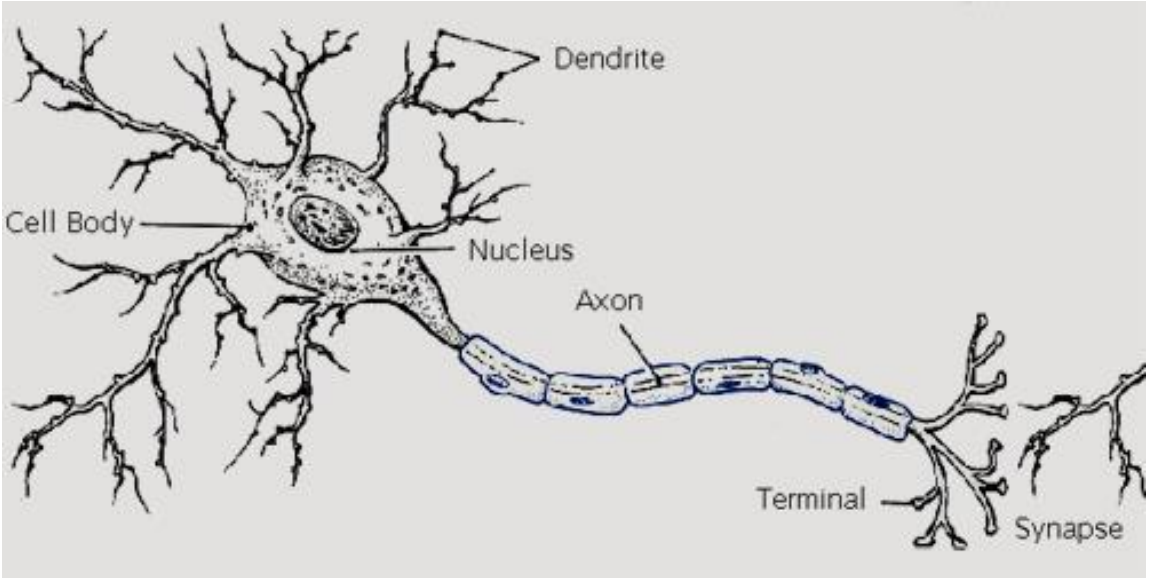

Electrical excitability of cells is possible because the movement of a few charges controls the flow of many charges.

Excitation (computed)

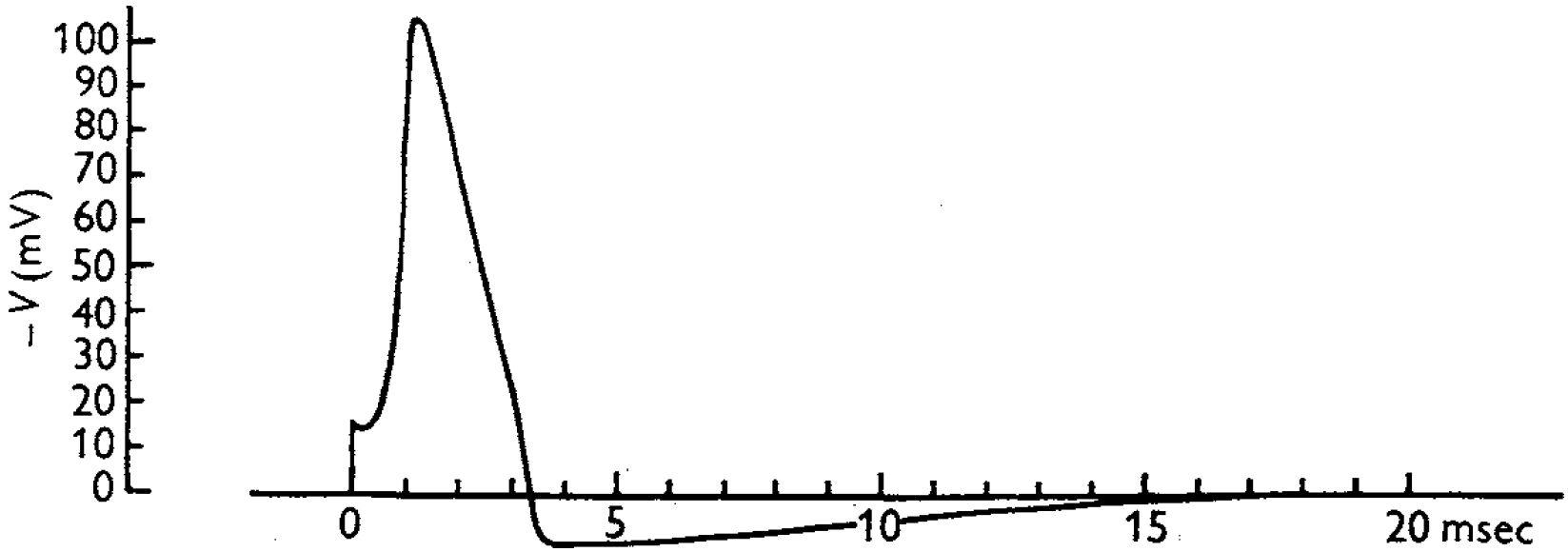

$$I = C_{\mathrm{M}}\dot{V} + \bar{g}_{\mathrm{K}} n^4 (V - V_{\mathrm{K}}) + \bar{g}_{\mathrm{Na}} m^3 h (V - V_{\mathrm{Na}}) + \bar{g}_{\mathrm{l}} (V - V_{\mathrm{l}})$$

Hodgkin and Huxley (1952, Fig. 13, Eq. 26)

The Action Potential

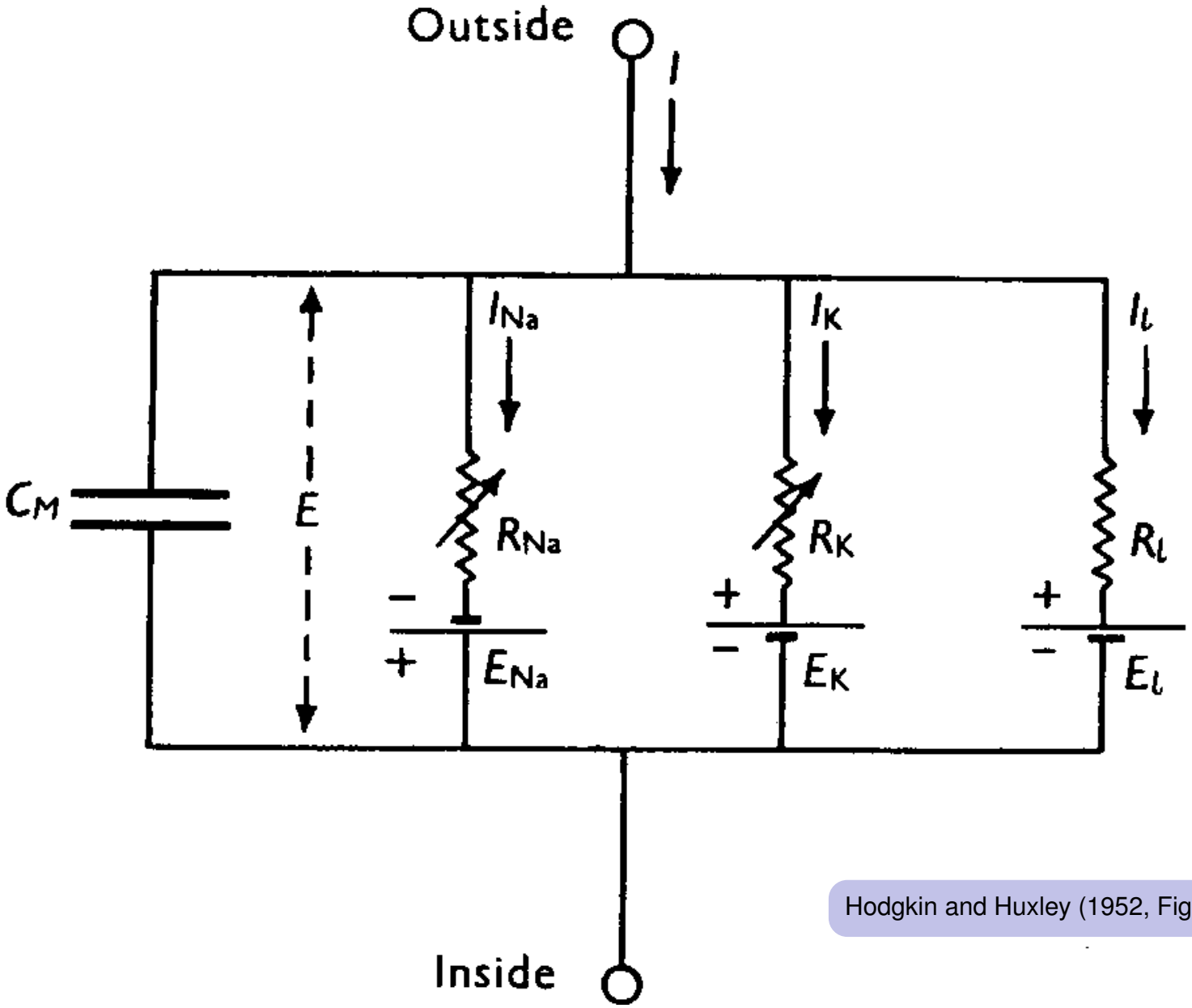

Hodgkin and Huxley (1952, Fig. 1)

The Action Potential

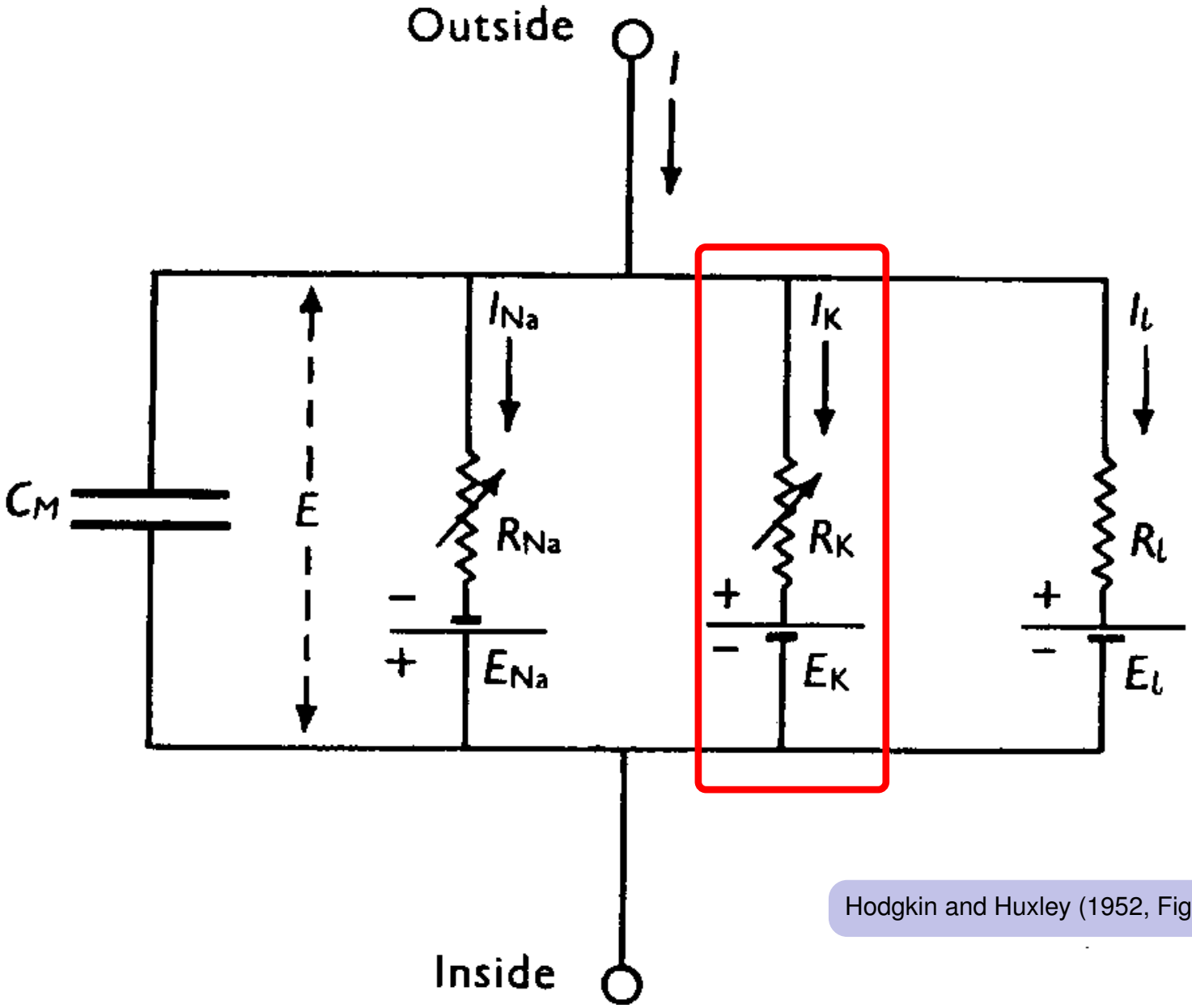

Hodgkin and Huxley (1952, Fig. 1)

The Action Potential

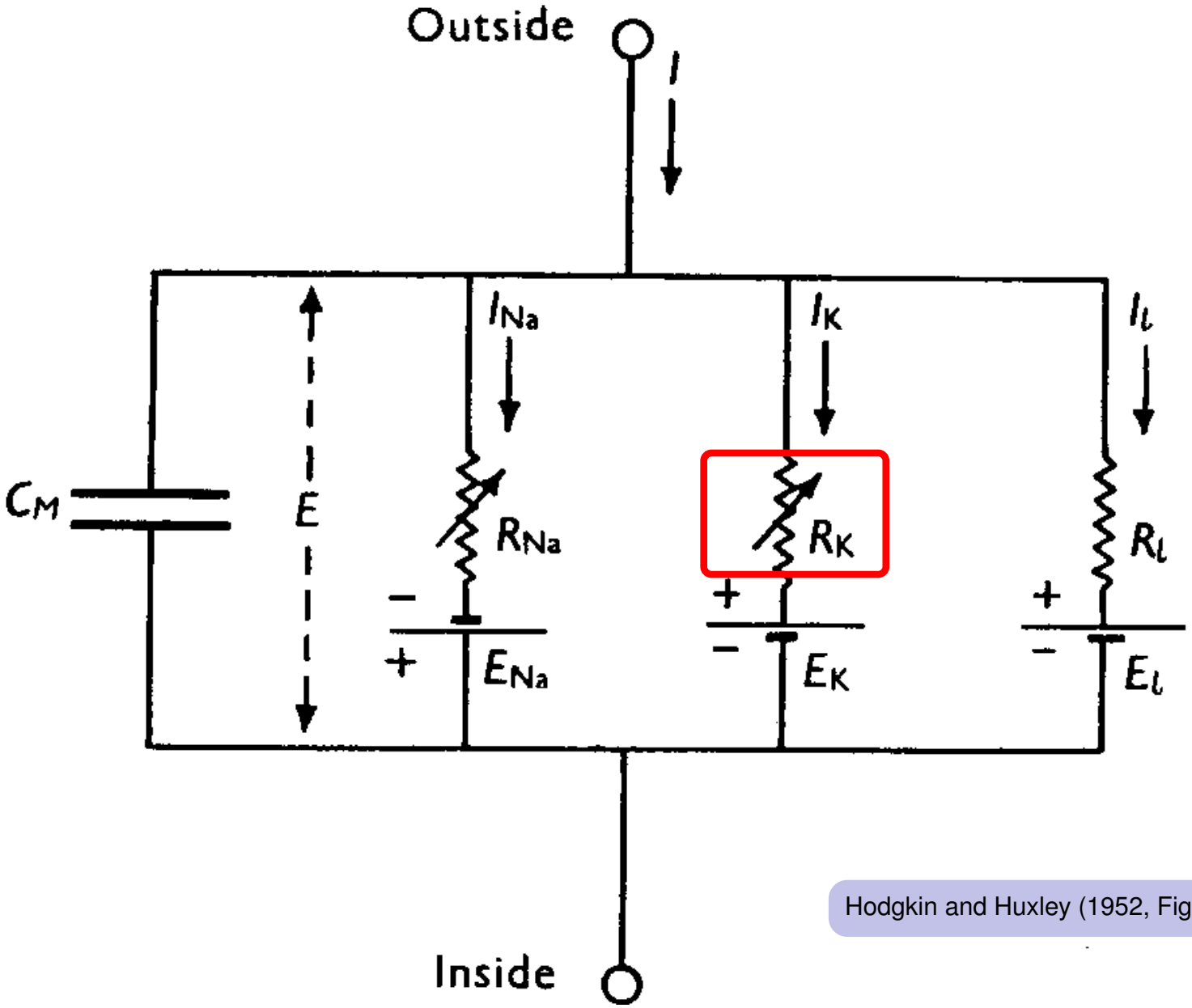

Hodgkin and Huxley (1952, Fig. 1)

Voltage Gated K^+ Currents

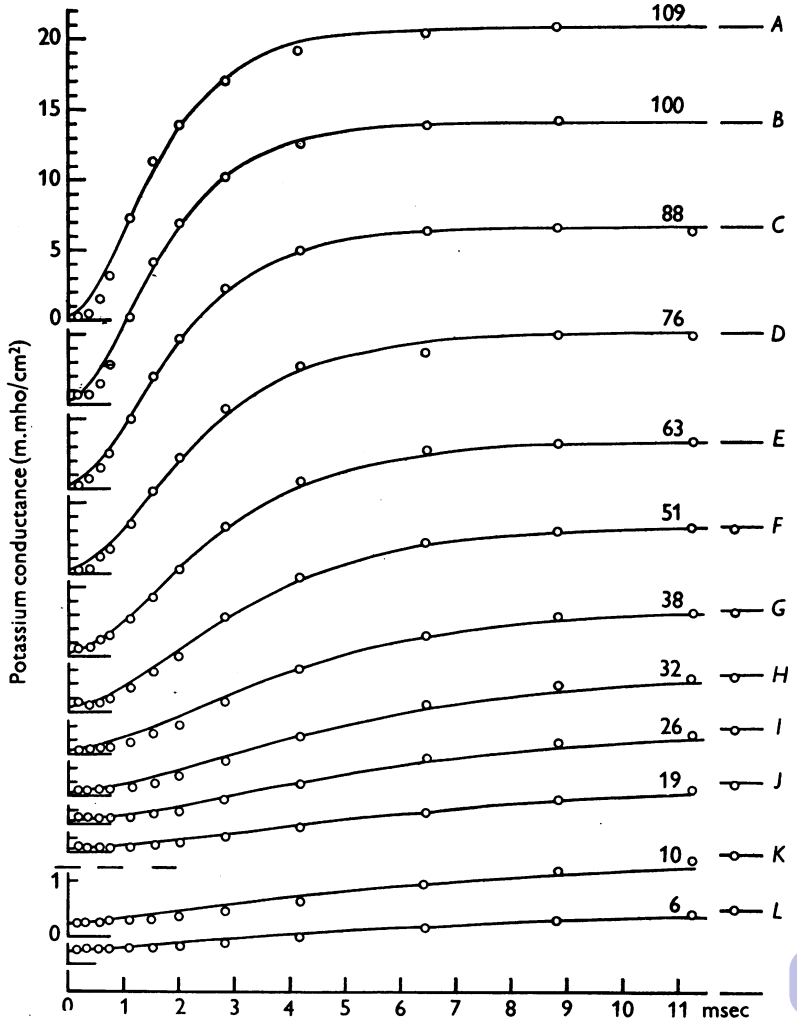

Hodgkin and Huxley (1952, Fig. 3)

$$g_{\mathrm{K}}(t) = g_{\mathrm{K}\infty}\left\{1 - \left[1 - \sqrt[4]{g_{\mathrm{K}0}/g_{\mathrm{K}\infty}}\right]\exp(-t/\tau_n)\right\}^4$$

Voltage-sensor displacement

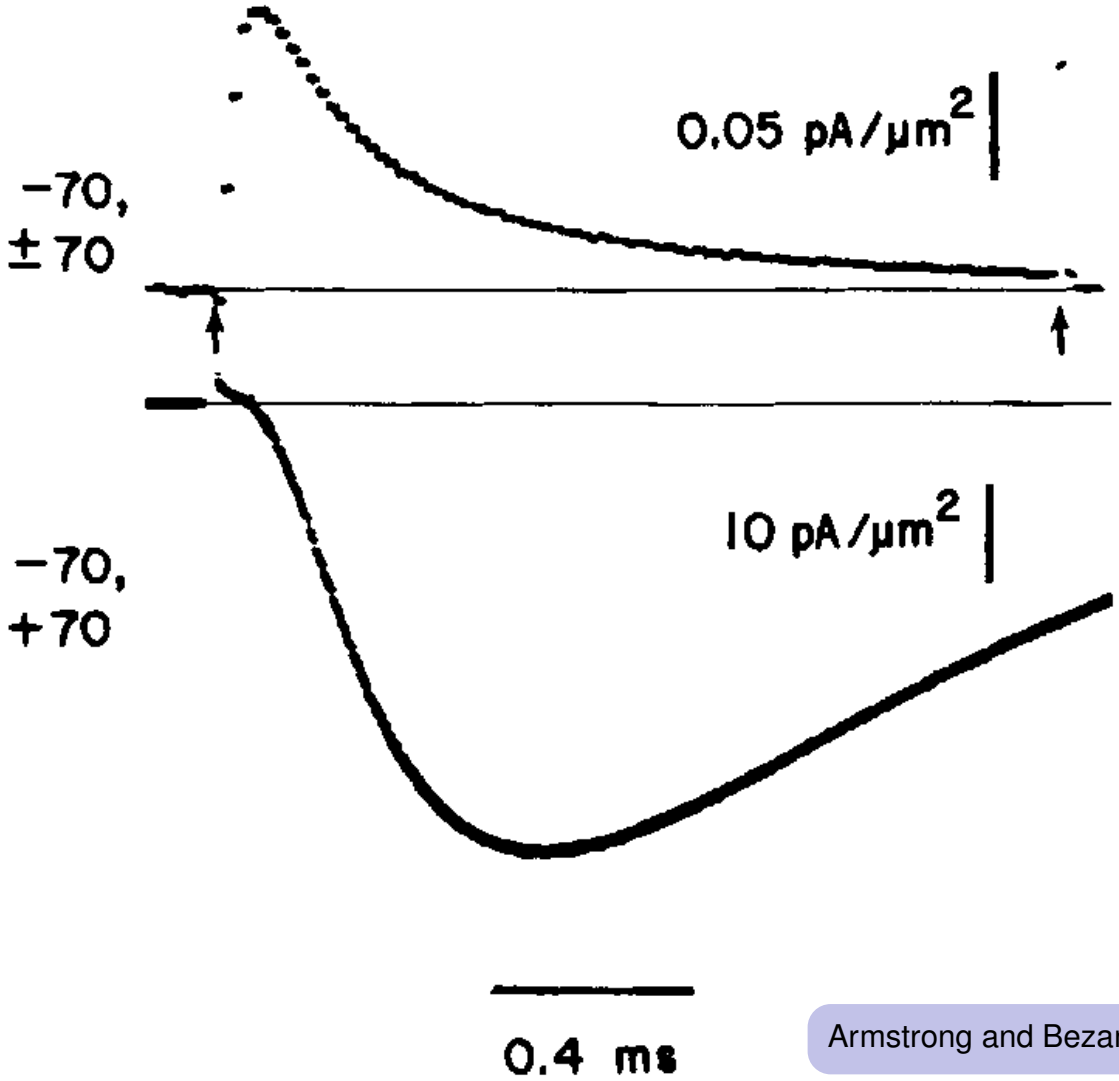

Armstrong and Bezanilla (1973, Fig. 2)

Topology

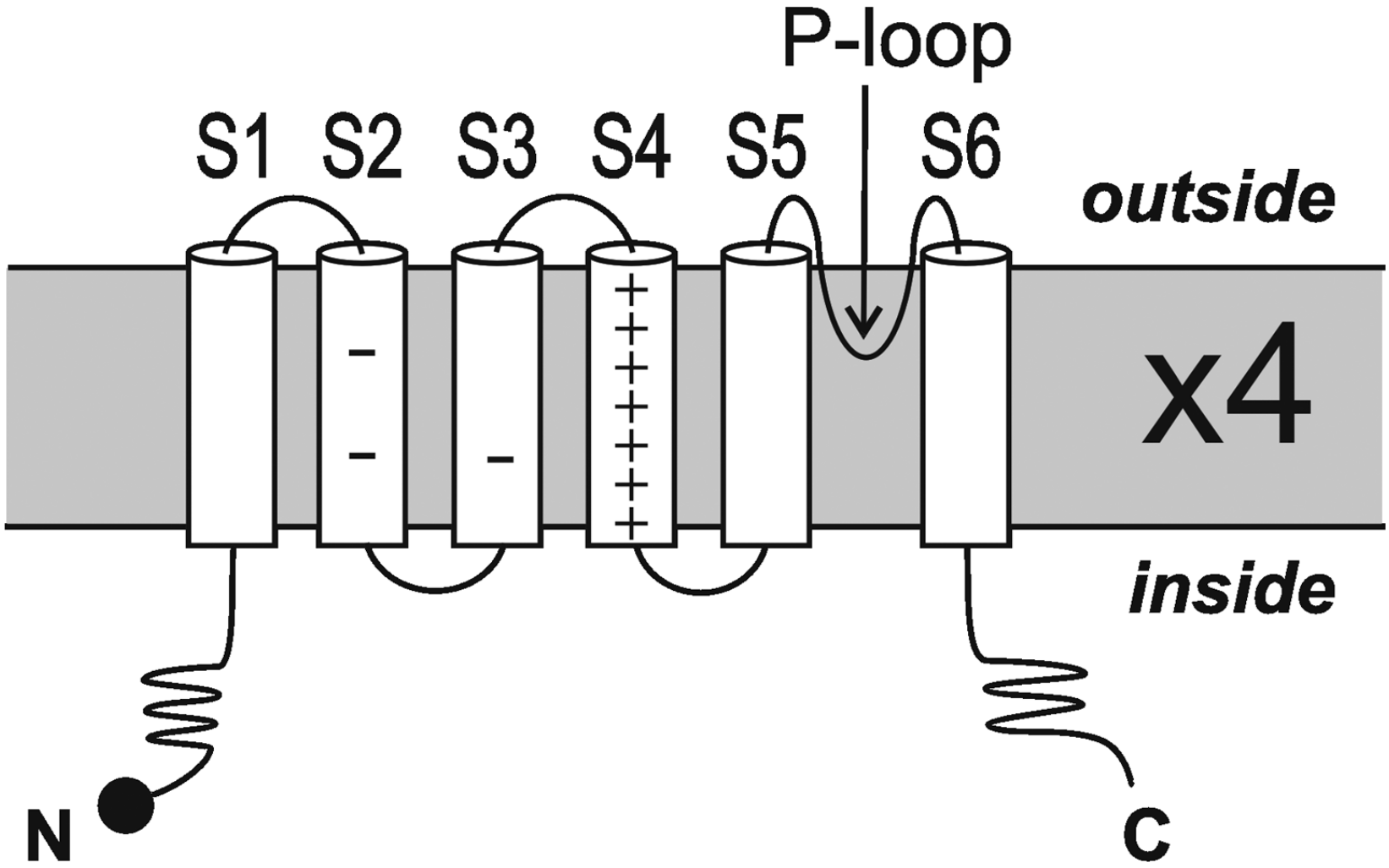

Gandhi and Isacoff (2002, Fig. 1a)

Topology

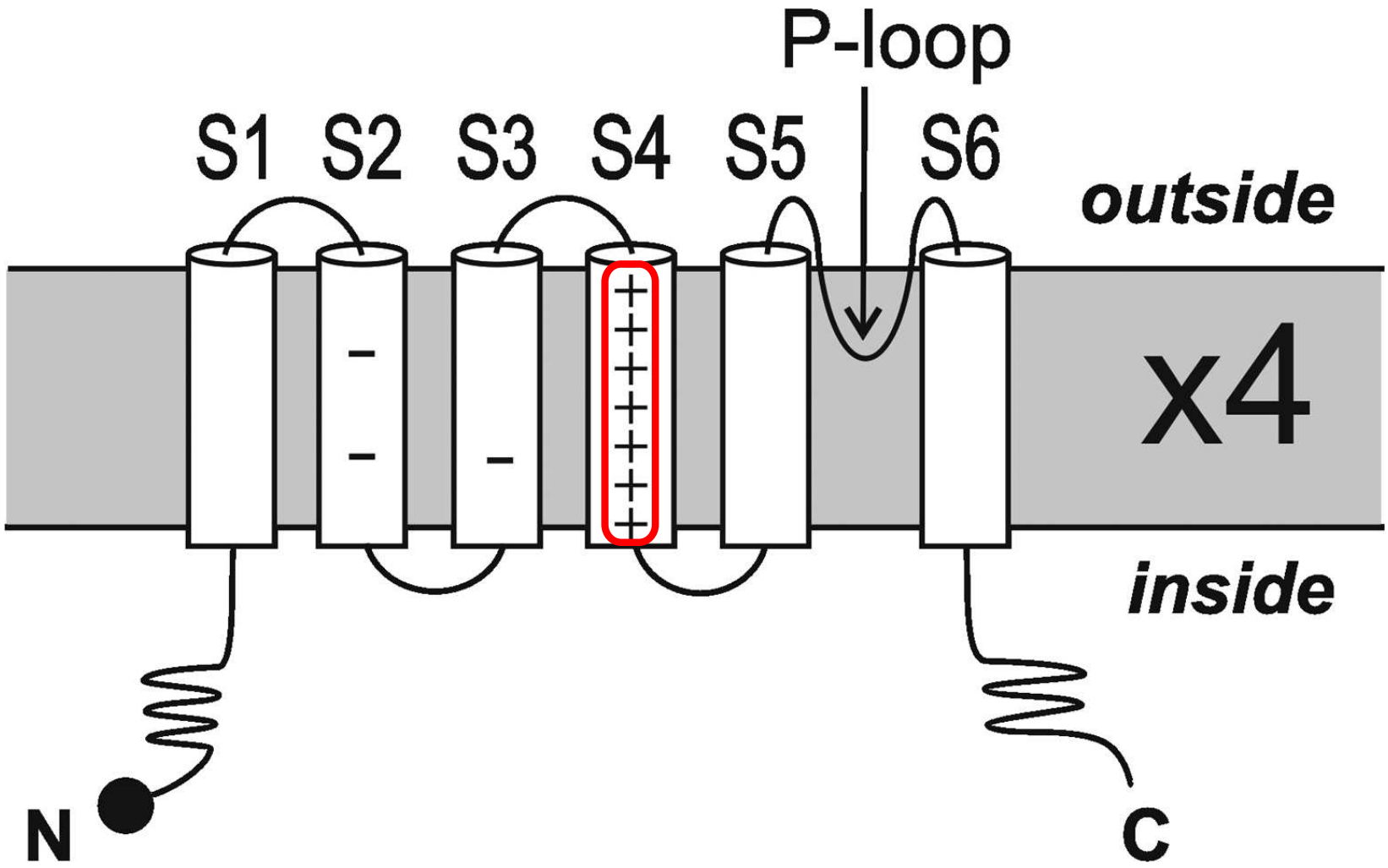

Gandhi and Isacoff (2002, Fig. 1a)

Structure

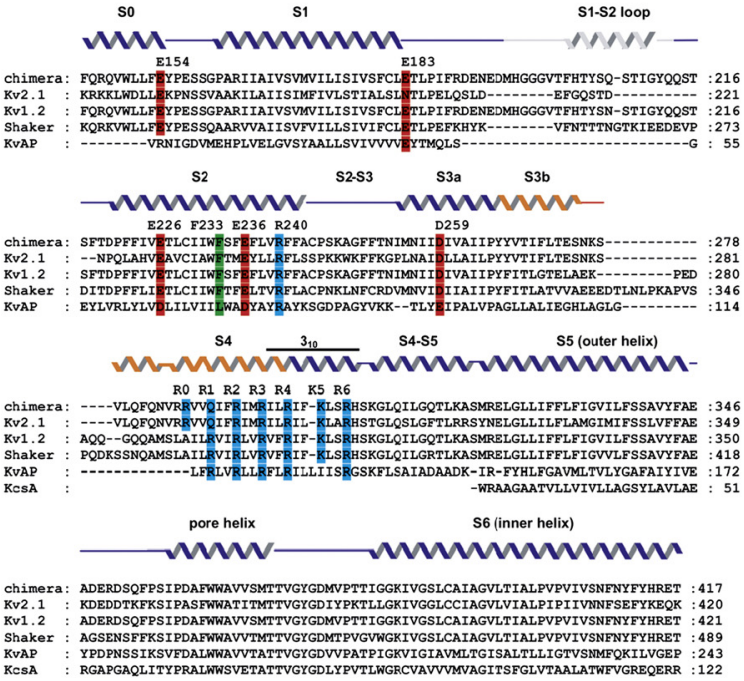

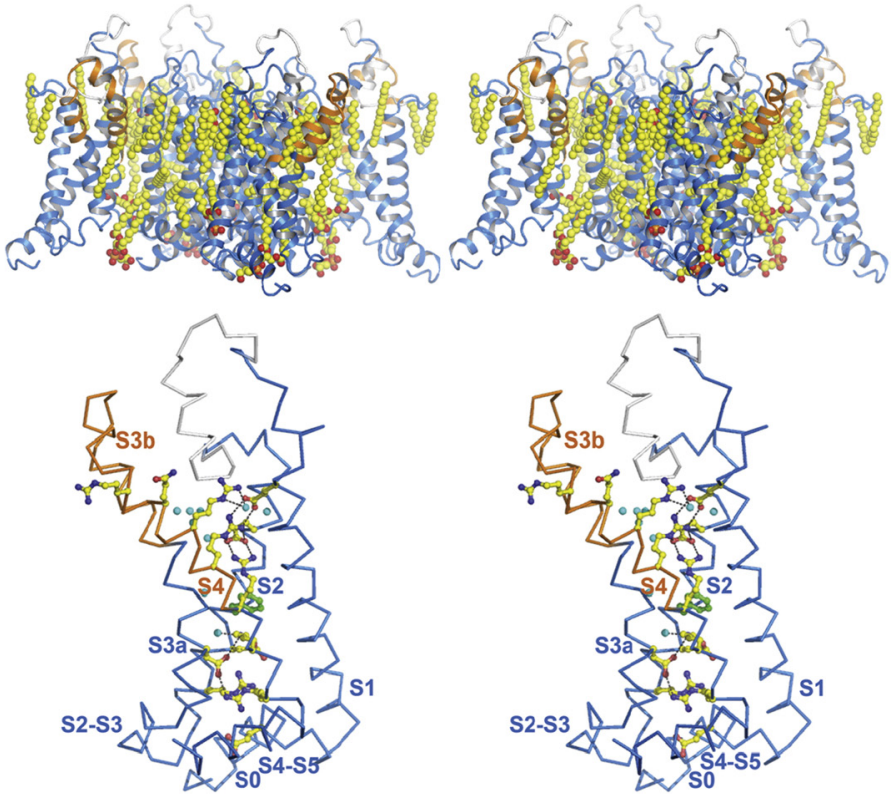

Tao and MacKinnon (2008, Fig. 1)

Molecular Dynamics

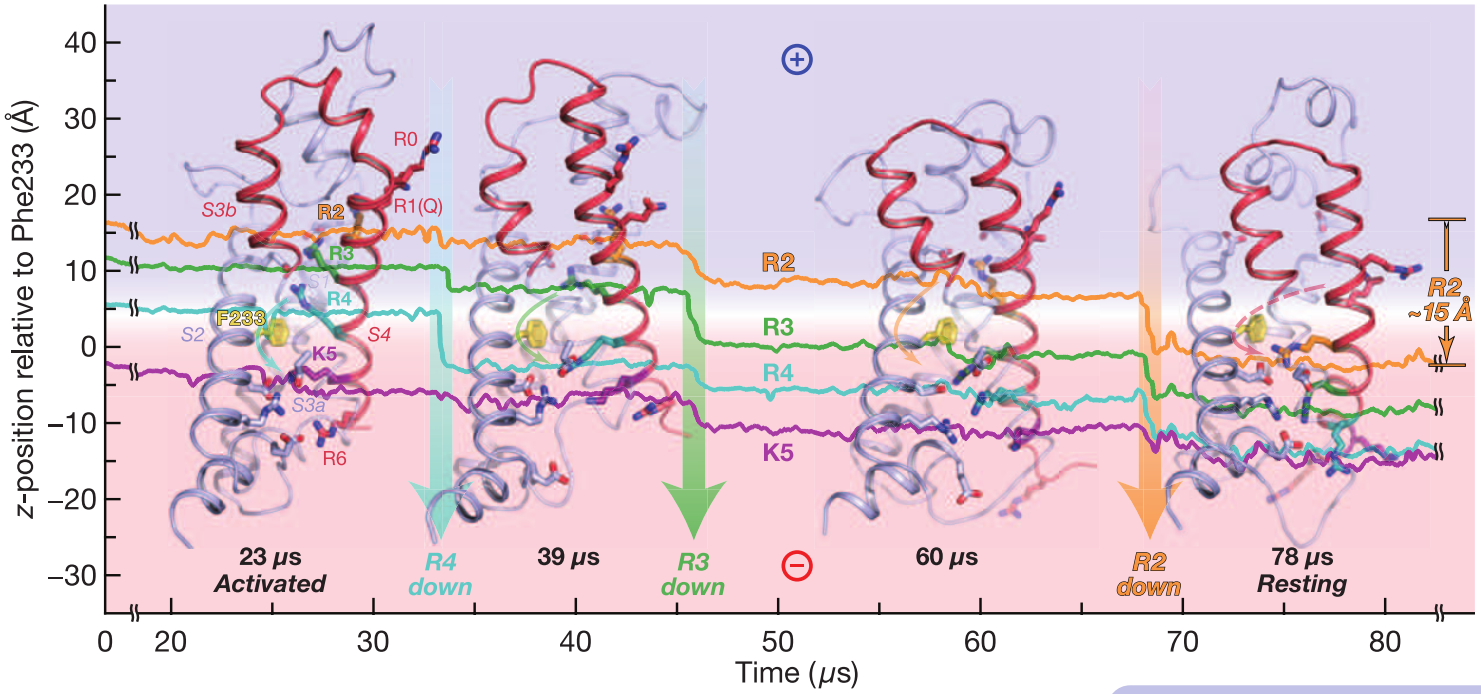

Jensen et al. (2012, Fig. 1B)

Geometry: Radial

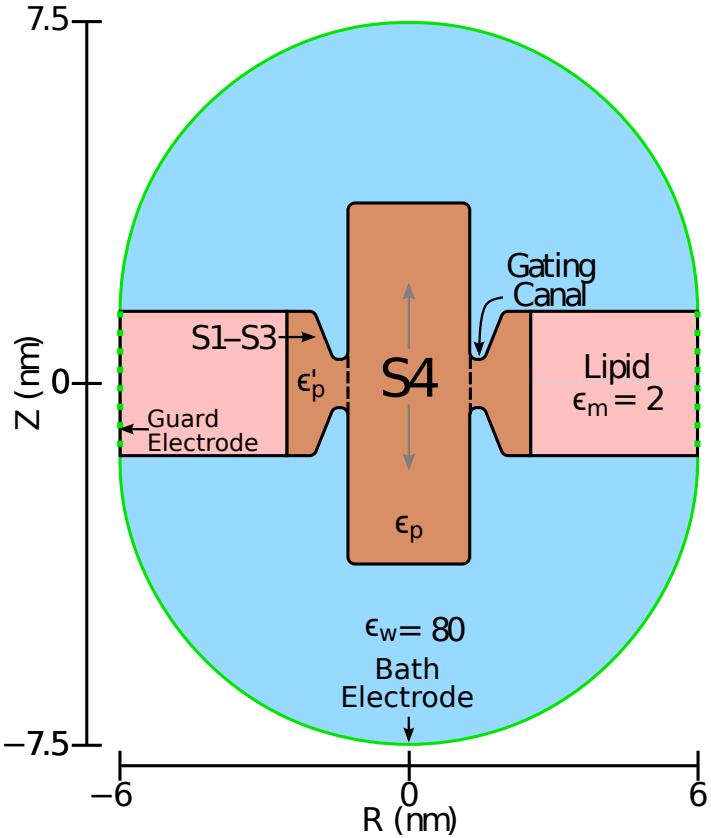

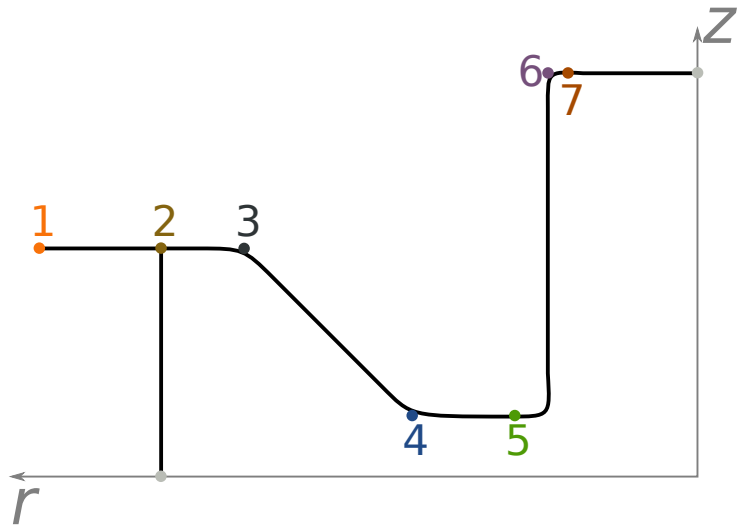

Model		1	2	3	4	5	6	7
α	r	6.0	2.532	1.966	1.566	1.466	1.266	1.0
	z	1.5	1.5	1.5	0.5015	0.5015	3.7515	3.7515
3_{10}	r	6.0	2.492	1.946	1.546	1.446	1.246	0.98
	z	1.5	1.5	1.5	0.602	0.602	4.602	4.602

Peyser and Nonner (2012a, Fig. 1)

Geometry: 3d

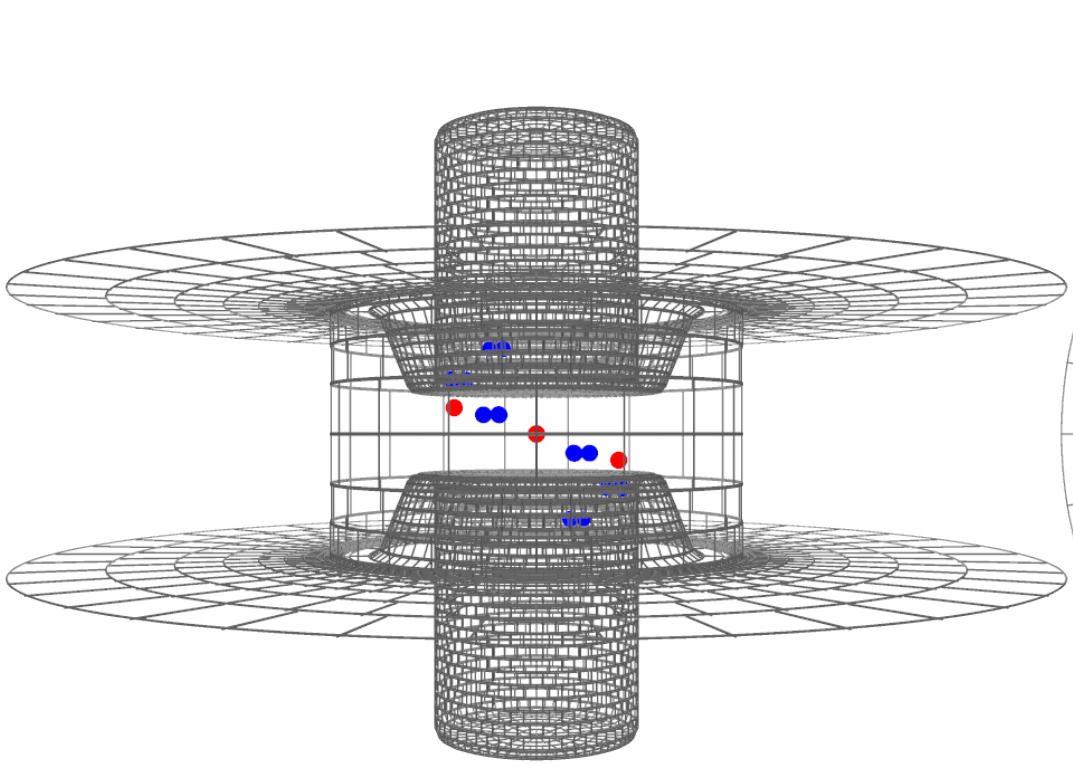

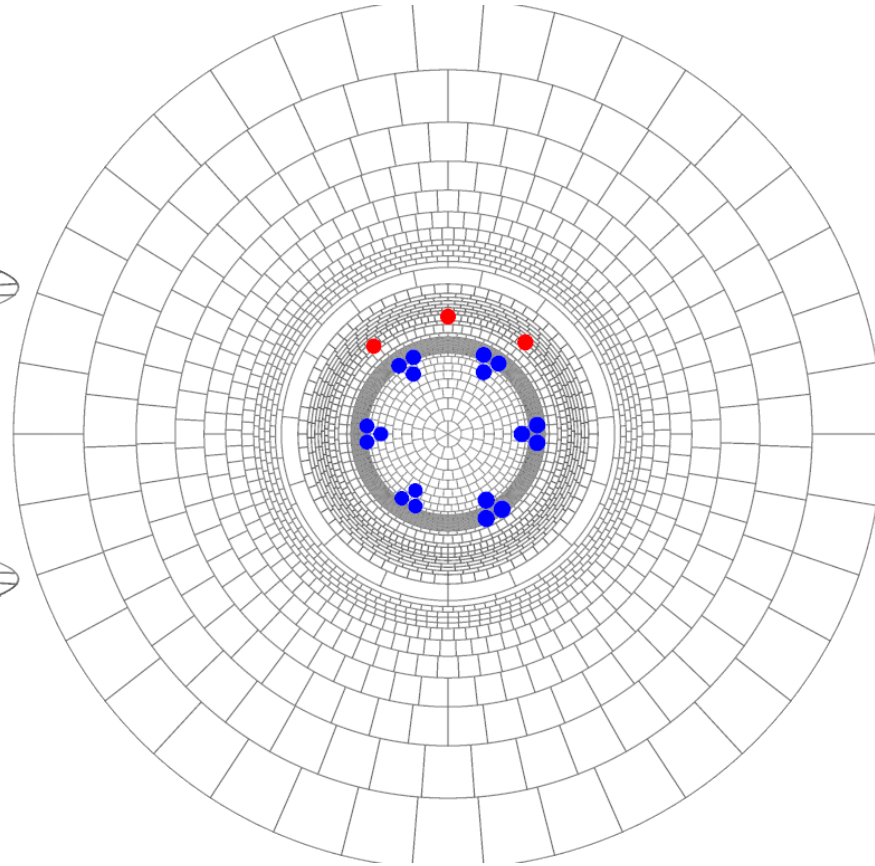

Peyser and Nonner (2012a, Fig. 2)

Basis for Induced Charge Calculation

JÜLICH FORSCHUNGSZENTRUM

Electric field in dielectric

Continuity of Displacement

$$\epsilon_1 \mathbf{E}_1^{\perp} = \epsilon_2 \mathbf{E}_2^{\perp}$$

Gauss' Law

$$\mathbf{E}_1^{\perp} + \frac{\sigma}{\epsilon_0}\mathbf{n} = \mathbf{E}_2^{\perp}$$

Surface Thickness

$$\mathbf{E}^{\perp} = \frac{\mathbf{E}_1^{\perp} + \mathbf{E}_2^{\perp}}{2}$$

Induced Charge Calculation

Charges in dielectric:

$$\rho^{\mathrm{i}}(\mathbf{r}) = \frac{1-\epsilon(\mathbf{r})}{\epsilon(\mathbf{r})}\rho^{\mathrm{s}}(\mathbf{r}) - \frac{\nabla\epsilon(\mathbf{r})}{\epsilon(\mathbf{r})} \cdot \epsilon_0 \mathbf{E}(\mathbf{r})$$

$$\rho^{\mathrm{e}}(\mathbf{r}) = \frac{\rho^{\mathrm{s}}(\mathbf{r})}{\epsilon(\mathbf{r})}.$$

Matrix equations:

$$4\pi\epsilon_0\ \mathbf{E}(\mathbf{r}) = \sum_k q_k^{\mathrm{e}} \frac{\mathbf{r}-\mathbf{r}_k}{|\mathbf{r}-\mathbf{r}_k|^3} + \int_{\mathcal{B}} \sigma^{\mathrm{i}}(\mathbf{r}') \frac{\mathbf{r}-\mathbf{r}'}{|\mathbf{r}-\mathbf{r}'|^3}\, da' + \int_{\mathcal{E}} \sigma^{\mathrm{e}}(\mathbf{r}') \frac{\mathbf{r}-\mathbf{r}'}{|\mathbf{r}-\mathbf{r}'|^3}\, da'$$

$$4\pi\epsilon_0\ V(\mathbf{r}) = \sum_k q_k^{\mathrm{e}} \frac{1}{|\mathbf{r}-\mathbf{r}_k|} + \int_{\mathcal{B}} \sigma^{\mathrm{i}}(\mathbf{r}') \frac{1}{|\mathbf{r}-\mathbf{r}'|}\, da' + \int_{\mathcal{E}} \sigma^{\mathrm{e}}(\mathbf{r}') \frac{1}{|\mathbf{r}-\mathbf{r}'|}\, da'$$

$$\sigma^{\mathrm{i}}(\mathbf{r}) = -\frac{\Delta\epsilon(\mathbf{r})}{\bar{\epsilon}(\mathbf{r})}\, \epsilon_0\, \mathbf{n}(\mathbf{r}) \cdot \mathbf{E}(\mathbf{r})$$

Discretization

JÜLICH FORSCHUNGSZENTRUM

Form

$$\mathbf{Ah} = \mathbf{c}$$

A_{ij} for dielectric surfaces i

$$[A_{ii}] = \frac{1}{a_i}\left(\int_{a_i} \frac{\mathbf{r}' \cdot n}{|\mathbf{r}'|^3}\, d\mathbf{r}' + 4\pi\right)$$

$$[A_{i\sim j}] = \frac{\Delta\epsilon_i}{\epsilon_i}\frac{1}{a_j}\int_{a_j} \frac{\mathbf{r}'_{ij} \cdot \mathbf{a}_i}{|\mathbf{r}'_{ij}|^3}\, d\mathbf{r}'_{ij}$$

$$[A_{ij}] = \frac{\Delta\epsilon_i}{\epsilon_i}\frac{\mathbf{r}_{ij} \cdot \mathbf{a}_i}{|\mathbf{r}_{ij}|^3}$$

Discretization

Form

$$\mathbf{A}\mathbf{h} = \mathbf{c}$$

A_{ij} for Dirichlet surfaces i

$$[A_{ii}] = \frac{1}{a_i} \int_{a_i} \frac{1}{\mathbf{r}} \, d\mathbf{r}$$

$$[A_{i\sim j}] = \frac{1}{a_j} \int_{a_j} \frac{1}{|\mathbf{r}_{ij}|} \, d\mathbf{r}_{ij}$$

$$[A_{ij}] = \frac{1}{|\mathbf{r}_{ij}|}$$

Discretization

Form

$$\mathbf{A}\mathbf{h} = \mathbf{c}$$

$\mathbf{h}_j$ for all surfaces

$$[\mathbf{h}_j] = \sigma_j a_j$$

Discretization

Form

$$\mathbf{A}\mathbf{h} = \mathbf{c}$$

$\mathbf{c}_i$ for dielectric surfaces i

$$[\mathbf{c}_i] = \frac{\Delta\epsilon_i}{\epsilon_i} \sum_k \frac{q_k}{\epsilon_k} \frac{\mathbf{r_{ik}} \cdot \mathbf{a}_i}{|\mathbf{r}_{ik}|^3}$$

Discretization

JÜLICH FORSCHUNGSZENTRUM

Form

$$\mathbf{A}\mathbf{h} = \mathbf{c}$$

$\mathbf{c}_i$ for dielectric surfaces i

$$[\mathbf{c}_i] = V_i - \sum_k \frac{q_k}{\epsilon_k} \frac{1}{|\mathbf{r}_{ik}|}$$

Oil Droplet

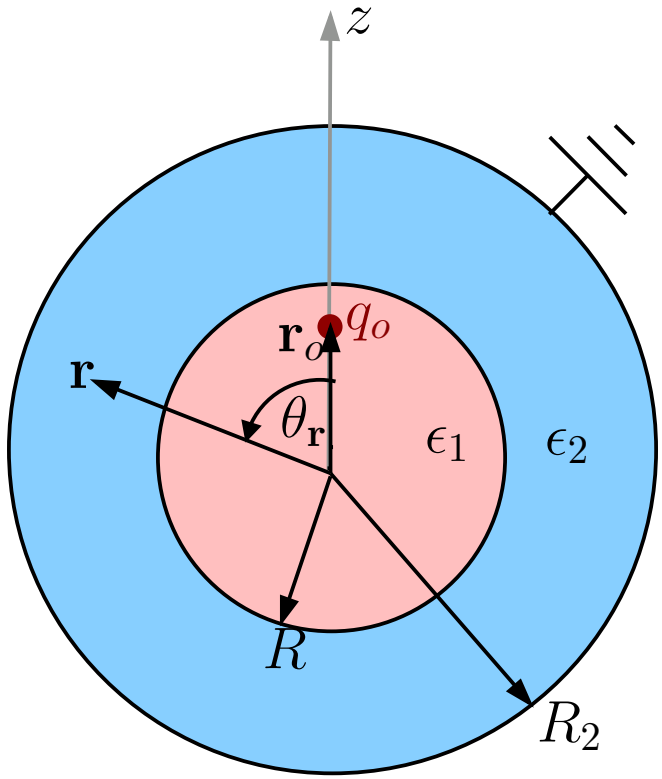

$r_o < R,\ r \leq R,\ R_2 \to \infty$

$$\phi_{11}(\mathbf{r}) = \frac{q_o}{4\pi\epsilon_0\epsilon_1}\left(\frac{1}{|\mathbf{r}-\mathbf{r_o}|} - \sum_{\ell=0}^{\infty}\frac{(\ell+1)(\epsilon_2-\epsilon_1)}{\ell\epsilon_1+(\ell+1)\epsilon_2}\cdot\frac{r_o^\ell r^\ell}{R^{2\ell+1}}P_\ell(\cos\theta_\mathbf{r})\right)$$

Oil Droplet

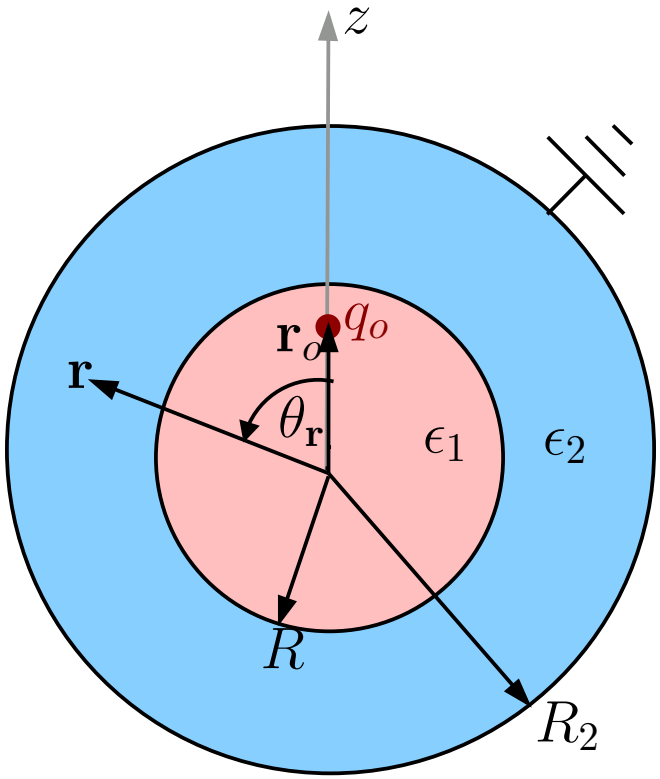

$r_o < R, r \geq R, R_2 \to \infty$

$$\phi_{12}(\mathbf{r}) = \frac{q_o}{4\pi\epsilon_o} \sum_{\ell=0}^{\infty} \frac{2\ell+1}{\ell\epsilon_1 + (\ell+1)\epsilon_2} \cdot \frac{r_o^\ell}{r^{\ell+1}} P_\ell(\cos\theta_\mathbf{r})$$

Oil Droplet

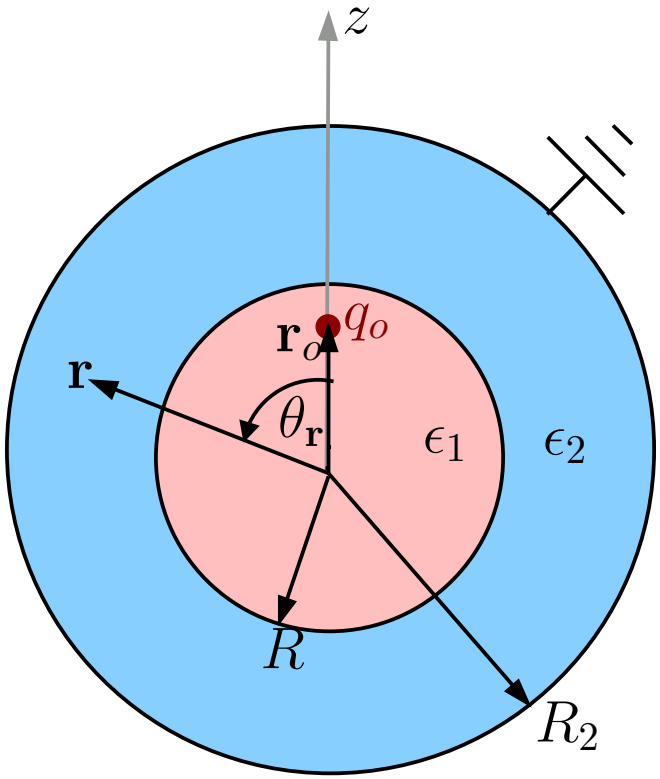

$r_o > R,\ r \leq R,\ R_2 \to \infty$

$$\phi_{11}(\mathbf{r}) = \frac{q_o}{4\pi\epsilon_0\epsilon_1}\left(\frac{1}{|\mathbf{r}-\mathbf{r_o}|} - \sum_{\ell=0}^{\infty}\frac{(\ell+1)(\epsilon_2-\epsilon_1)}{\ell\epsilon_1+(\ell+1)\epsilon_2}\cdot\frac{r_o^\ell r^\ell}{R^{2\ell+1}}P_\ell(\cos\theta_\mathbf{r})\right)$$

Oil Droplet

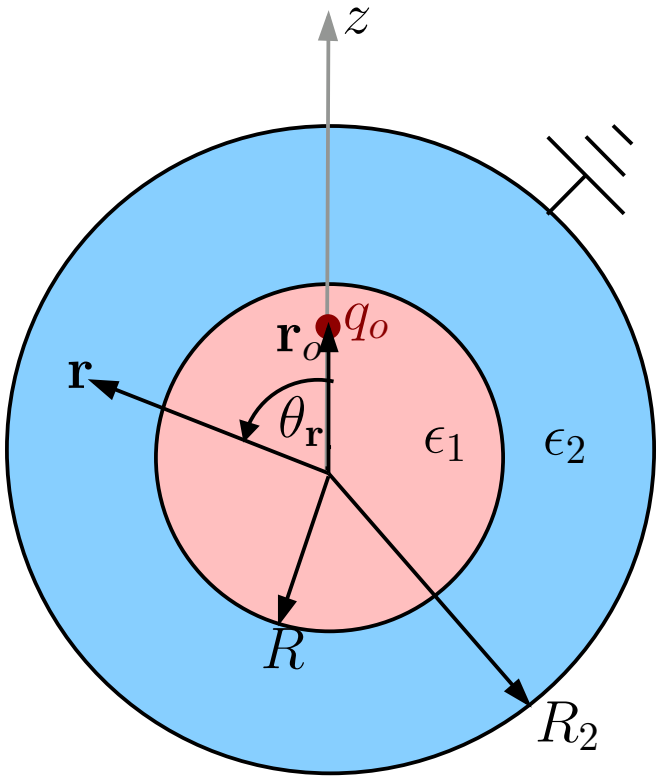

$r_o > R, r \geq R, R_2 \to \infty$

$$\phi_{12}(\mathbf{r}) = \frac{q_o}{4\pi\epsilon_o} \sum_{\ell=0}^{\infty} \frac{2\ell+1}{\ell\epsilon_1 + (\ell+1)\epsilon_2} \cdot \frac{r_o^\ell}{r^{\ell+1}} P_\ell(\cos\theta_\mathbf{r})$$

Oil Droplet

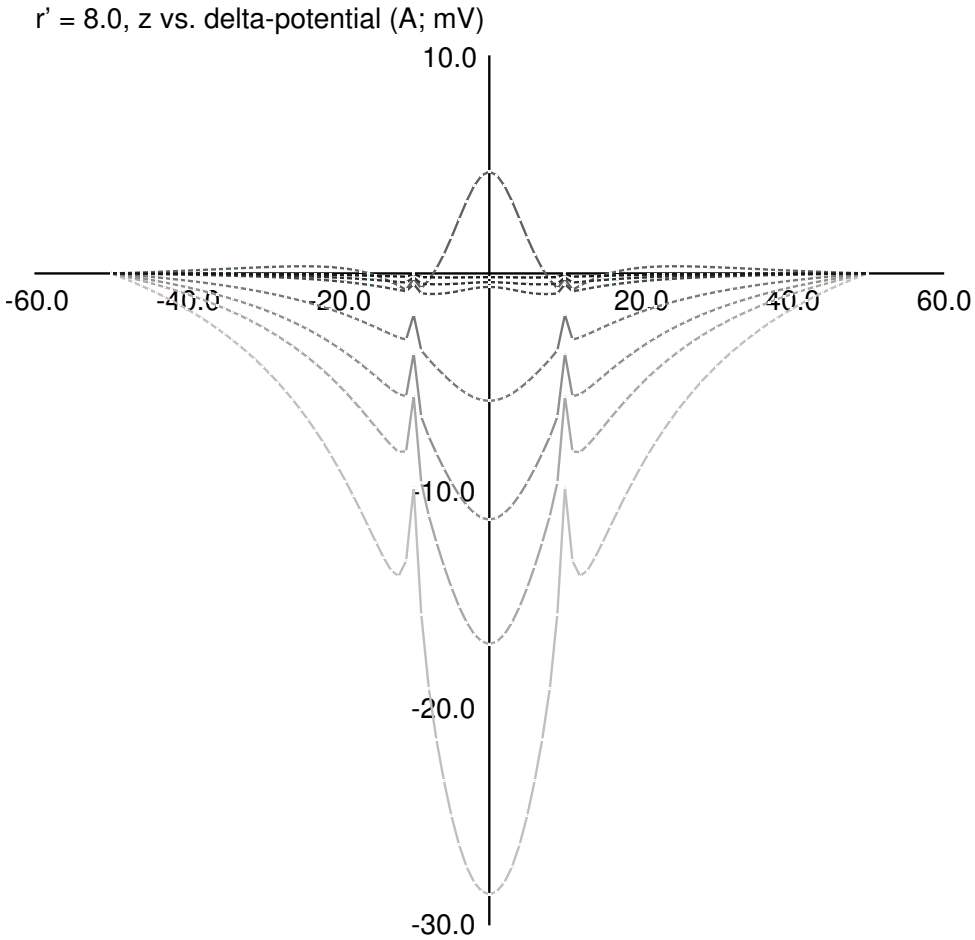
r' = 8.0, z vs. delta-potential (A; mV)
10.0
-10.0
-20.0
-30.0
-60.0
-40.0
-20.0
20.0
40.0
60.0

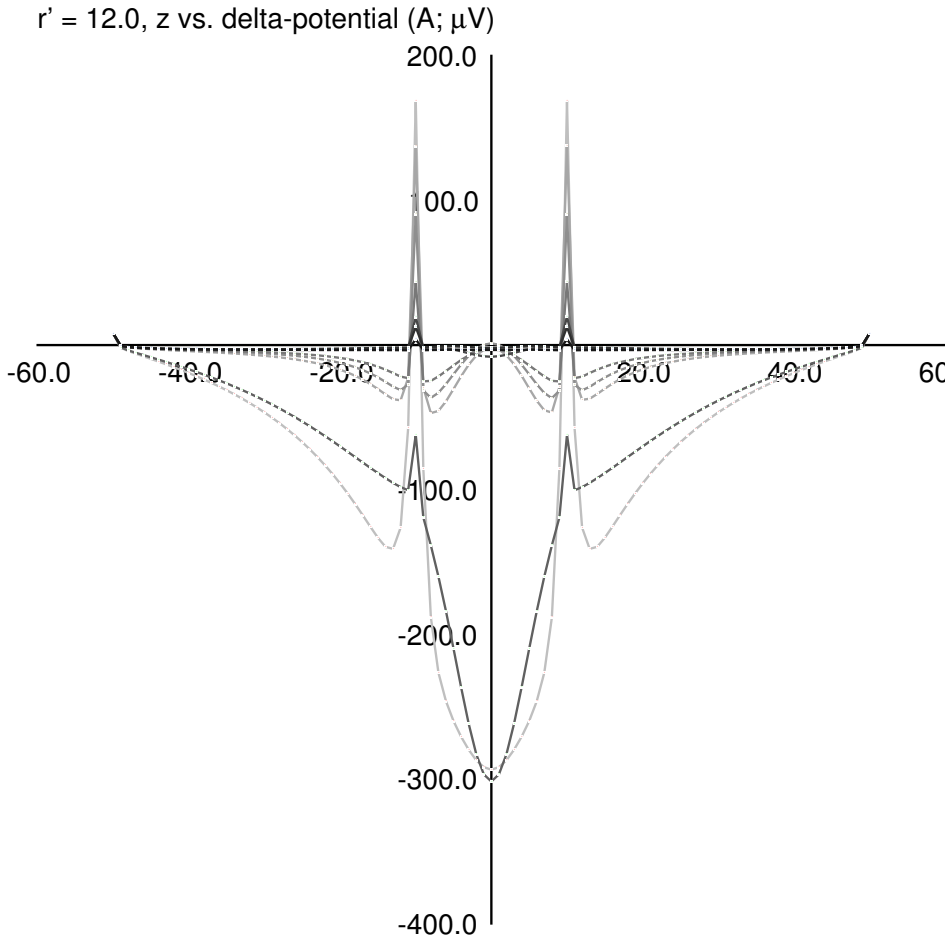
r' = 12.0, z vs. delta-potential (A; µV)
200.0
00.0
100.0
-200.0
-300.0
-400.0
-60.0
-40.0
-20.0
20.0
40.0

Geometry: Radial

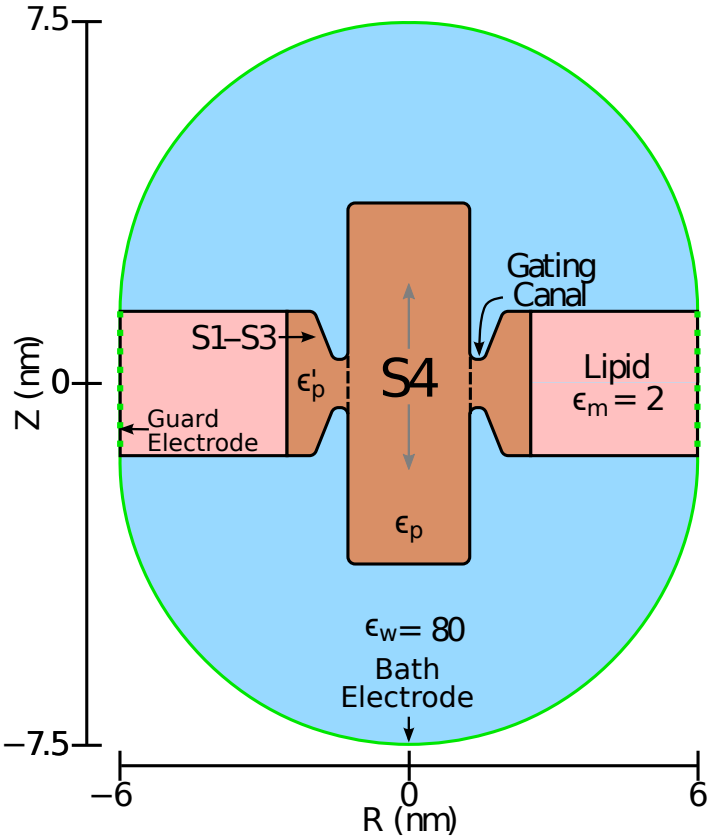

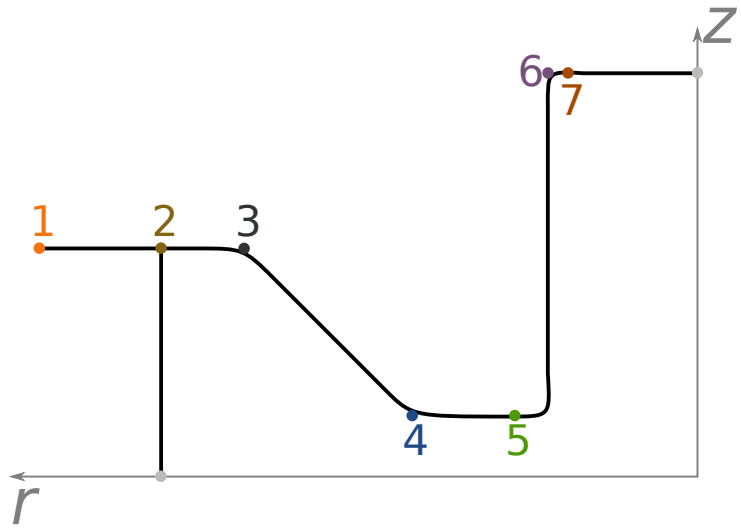

Model		1	2	3	4	5	6	7
α	r	6.0	2.532	1.966	1.566	1.466	1.266	1.0
	z	1.5	1.5	1.5	0.5015	0.5015	3.7515	3.7515
3_{10}	r	6.0	2.492	1.946	1.546	1.446	1.246	0.98
	z	1.5	1.5	1.5	0.602	0.602	4.602	4.602

Peyser and Nonner (2012a, Fig. 1)

Geometry: 3d

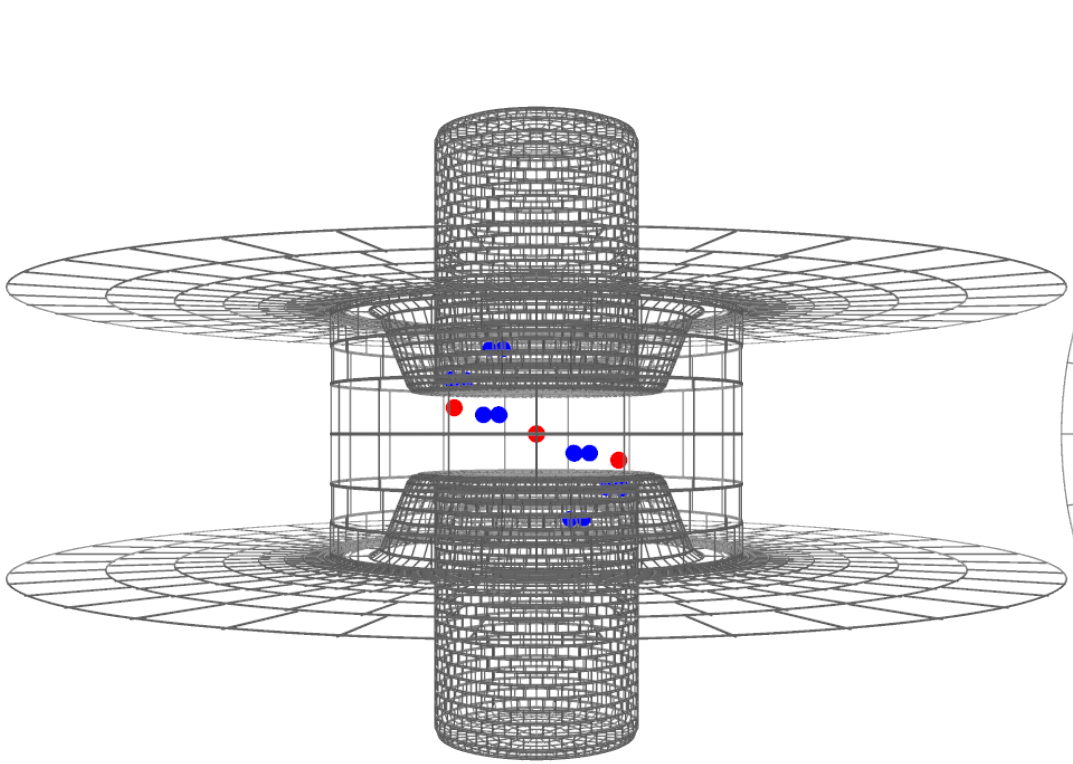

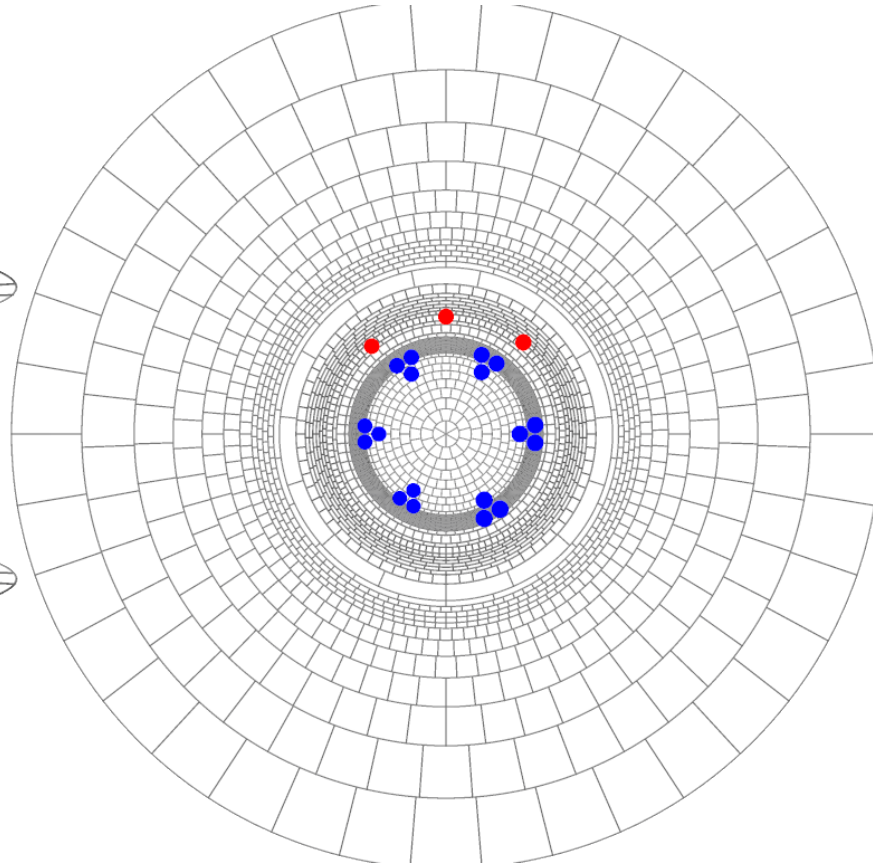

Peyser and Nonner (2012a, Fig. 2)

Gauss' Law

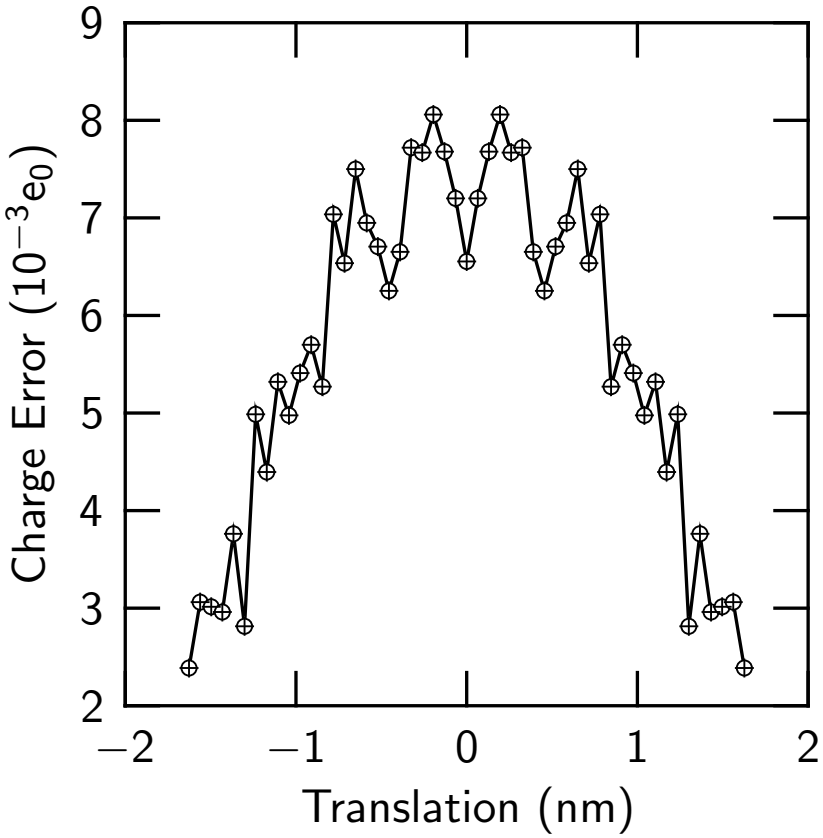

$$\oint_{\mathcal{S}} \epsilon(\mathbf{r})\,\epsilon_0 \mathbf{E}(\mathbf{r}) \cdot \mathbf{n}(\mathbf{r})\; da = \int_{\mathcal{V}} \rho^{\text{src}}(\mathbf{r})\; d\tau$$

$$Q_{\text{calc}} - Q_{\text{Gauss}} = -\sum_j \frac{\epsilon_{\text{p}}\epsilon_j}{\epsilon_j - \epsilon_{\text{p}}} \sigma^{\text{ind}} a_j - \sum_k q_k^{\text{src}}$$

Energetics

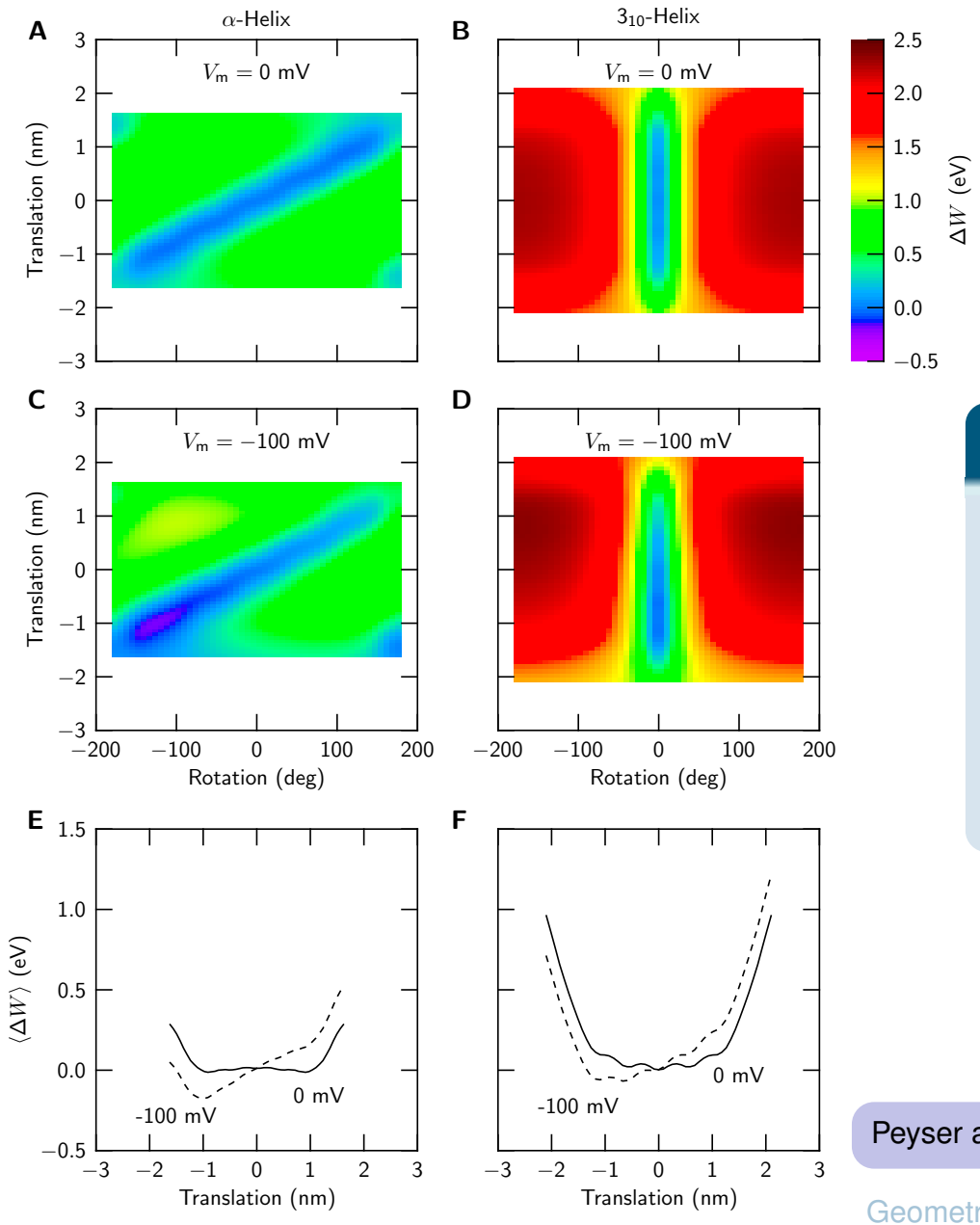

Partition function

$$\mathcal{Q} = \sum_i \exp(-\Delta W_i / k_B T)$$

$$P_i = \exp(-\Delta W_i / k_B T) / \mathcal{Q}$$

Peyser and Nonner 2012b

Output: Energy & Displacement

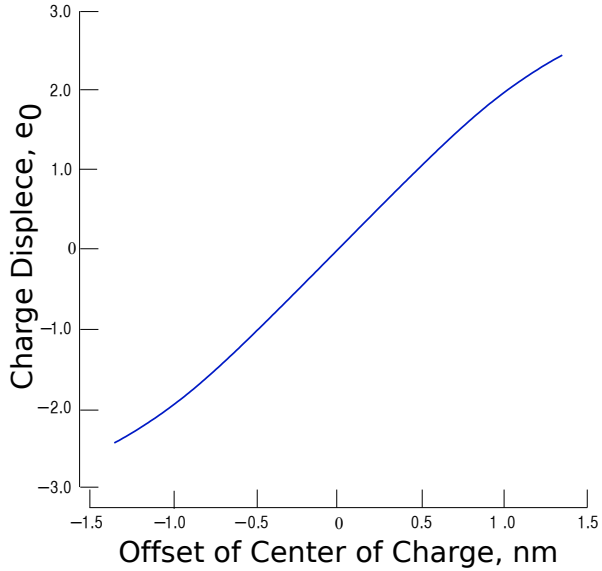

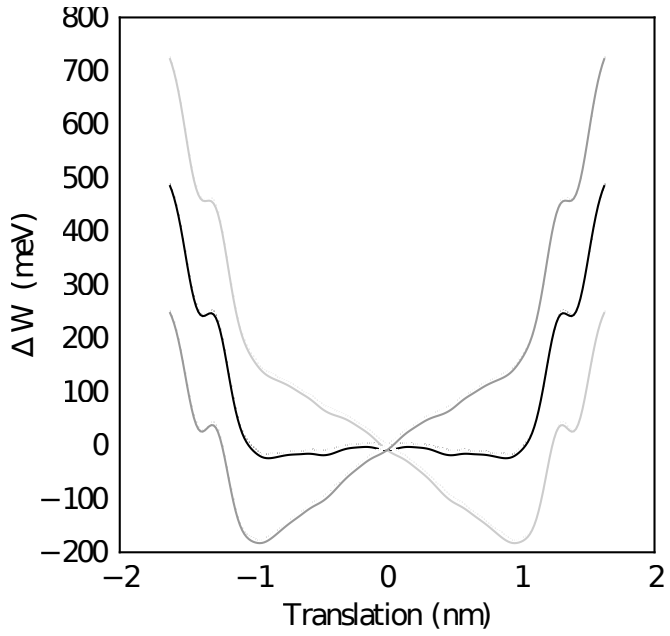

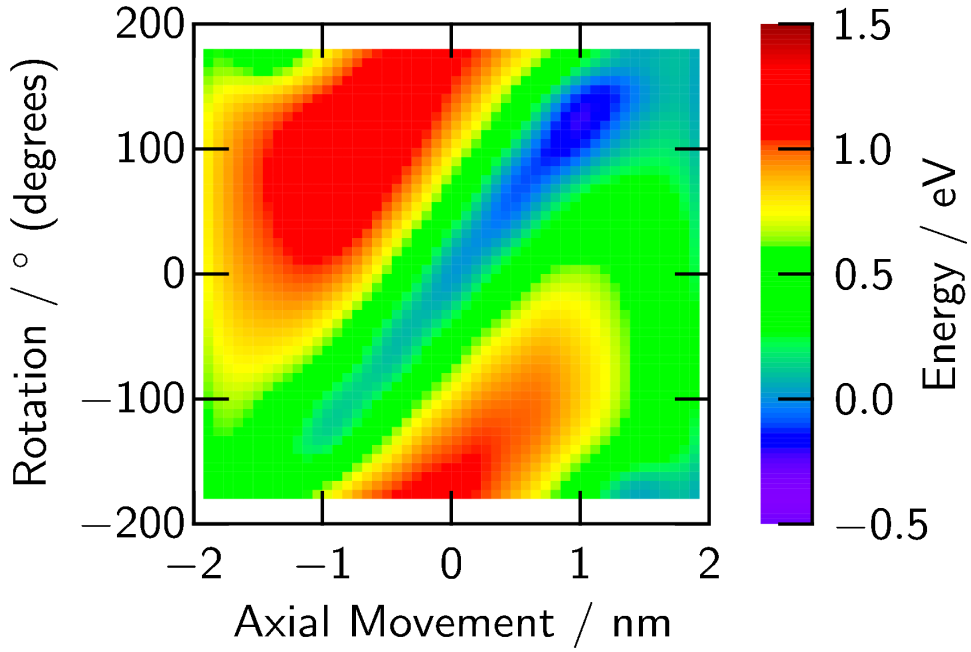

Shockley-Ramo Displacement

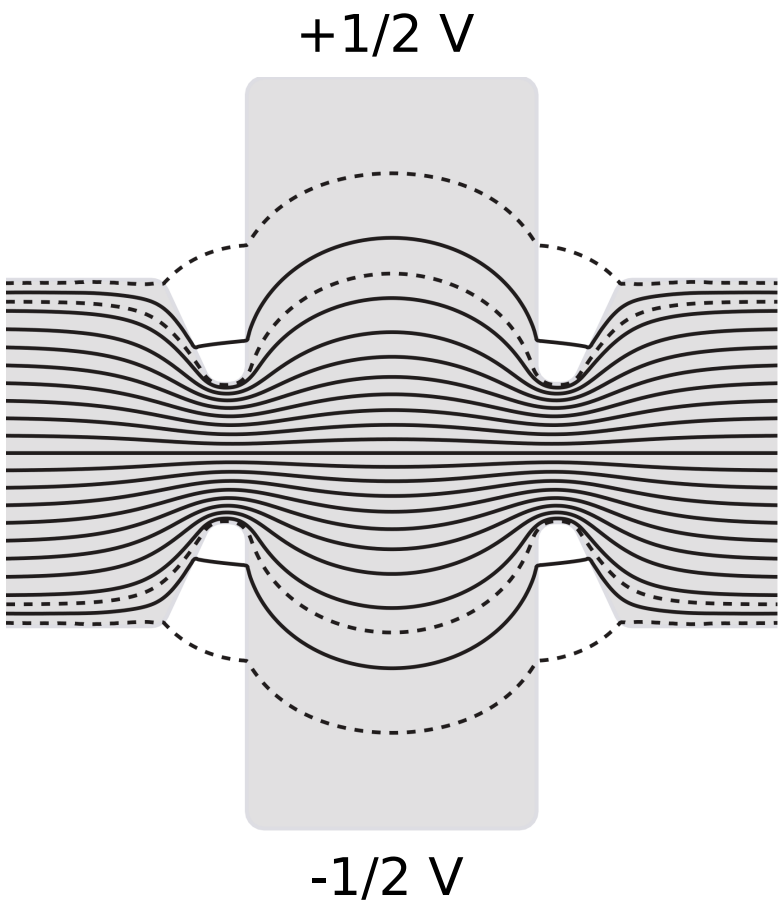

Shockley-Ramo Theorem (Integrated)

$$Q = -\sum_k q_k \; V_o(\mathbf{r}_k)/(1V)$$

Shockley-Ramo Displacement

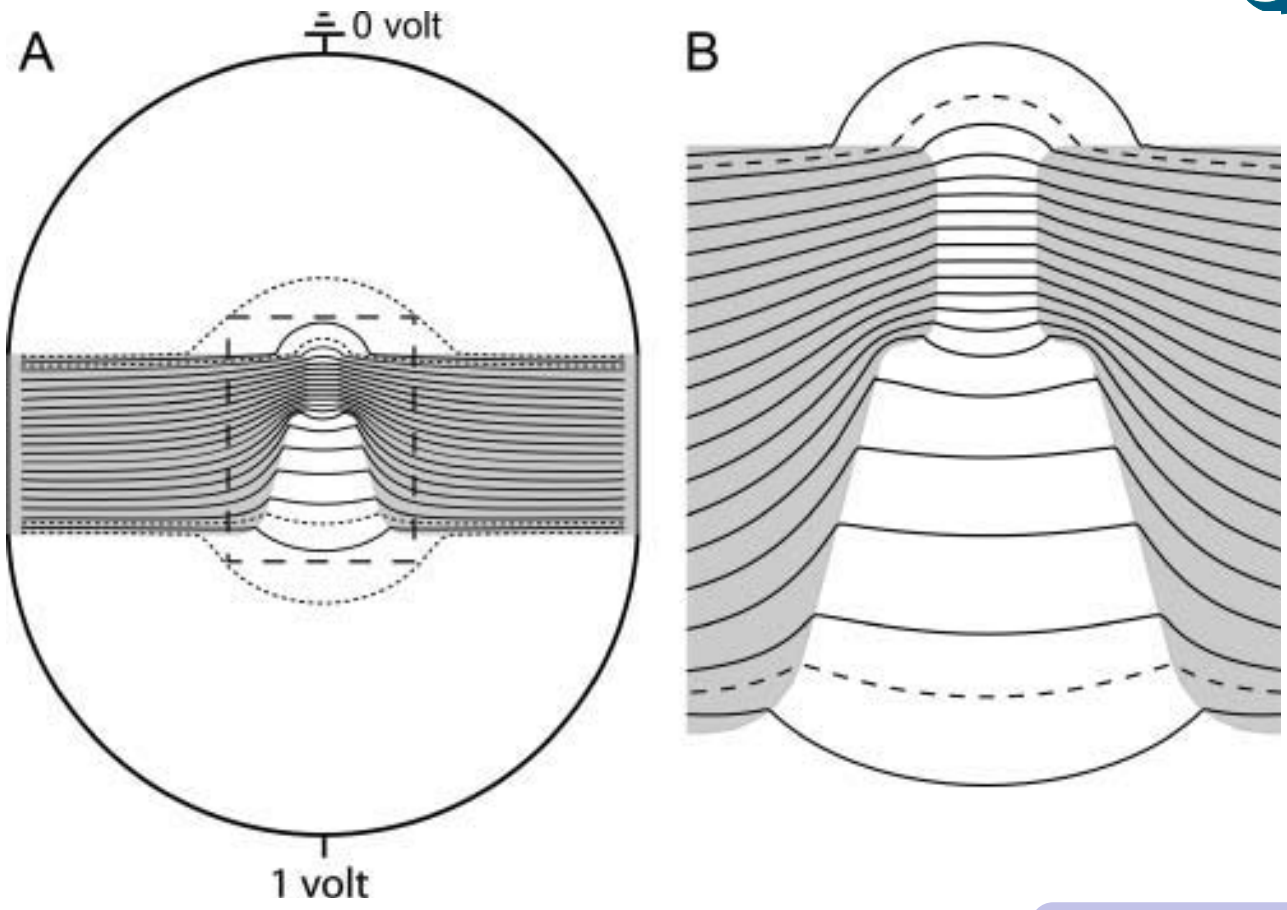

Nonner et al. (2004, Fig. 2)

Shockley-Ramo Theorem (Integrated)

$$Q = -\sum_k q_k \; V_o(\mathbf{r}_k)/(1\,V)$$

Engineering

Environment

Deuterostome (D) language: Postscript extended for numerics. Late-binding RPN, with data, operand and hash-table stacks.

History: 32-bit single-process OS9 $\Rightarrow$ OSX $\Rightarrow$ 64-bit parallel Linux.

Extensions

Structures	Bi-endian and Bi-word size.
Comms	Transport of hash-summed D executable objects transported by TCP, Unix sockets and MPI.
Parallelized	Numerical C operators were multithreaded, D procedures were multiprocessed, and program units were distributed across nodes with dependency-tracking D job server.
Libraries	Atlas BLAS and PETSc were integrated.
Numerics	Hand optimized.

Cluster

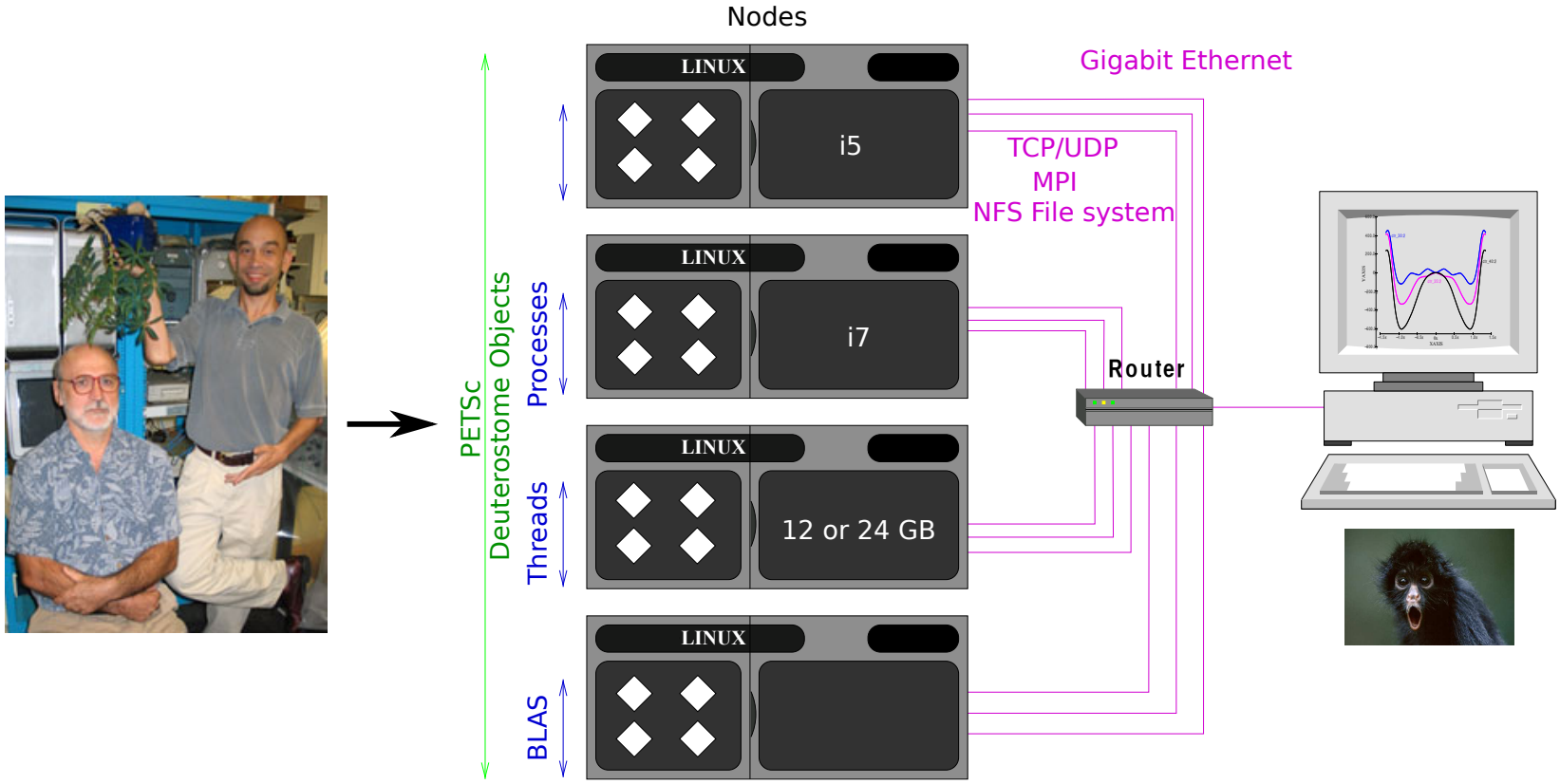

Cumulative speedup

$$\mathcal{O}(nodes) \times \mathcal{O}(cores/node) \times \sim 100 \text{ (software \& hardware)}$$

Shockley-Ramo Energetics

Instead of using force integration or change in potential for each charged particle, SR can be extended to energetic calculations:

$$W = \frac{1}{2} \sum_k q_k V^{V_\varepsilon = 0}(\mathbf{r}_k) - Q V_m$$

He (2001)

Then all results can be calculated from one SR energy calculation with $V_m = 0$, and one SR displacement calculation $V_m = 1$ V for each conformation.

This results in a $\mathcal{O}(\textit{voltage steps})$ speedup, after LU decomp.

Displacement: $\langle Q \rangle$

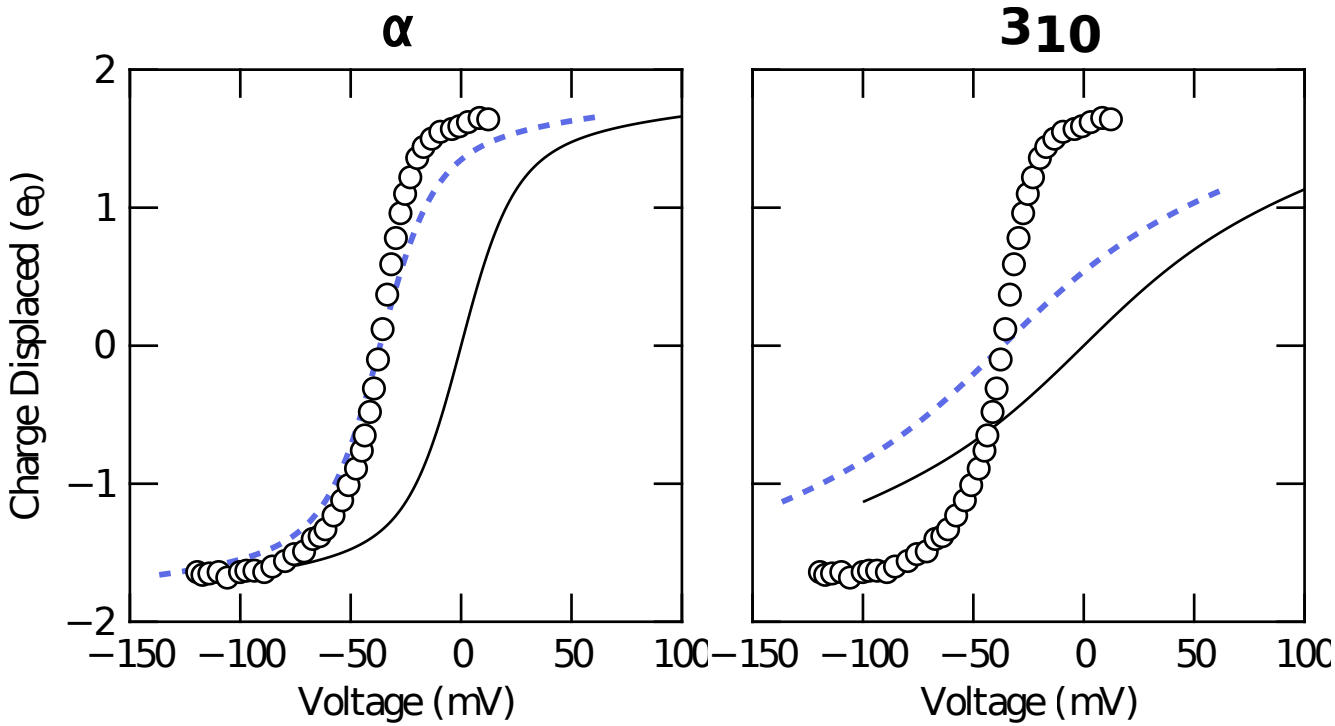

Peyser and Nonner (2012b, Fig. 3)

Seoh et al. (1996, Fig. 2)

Countercharge Geometry

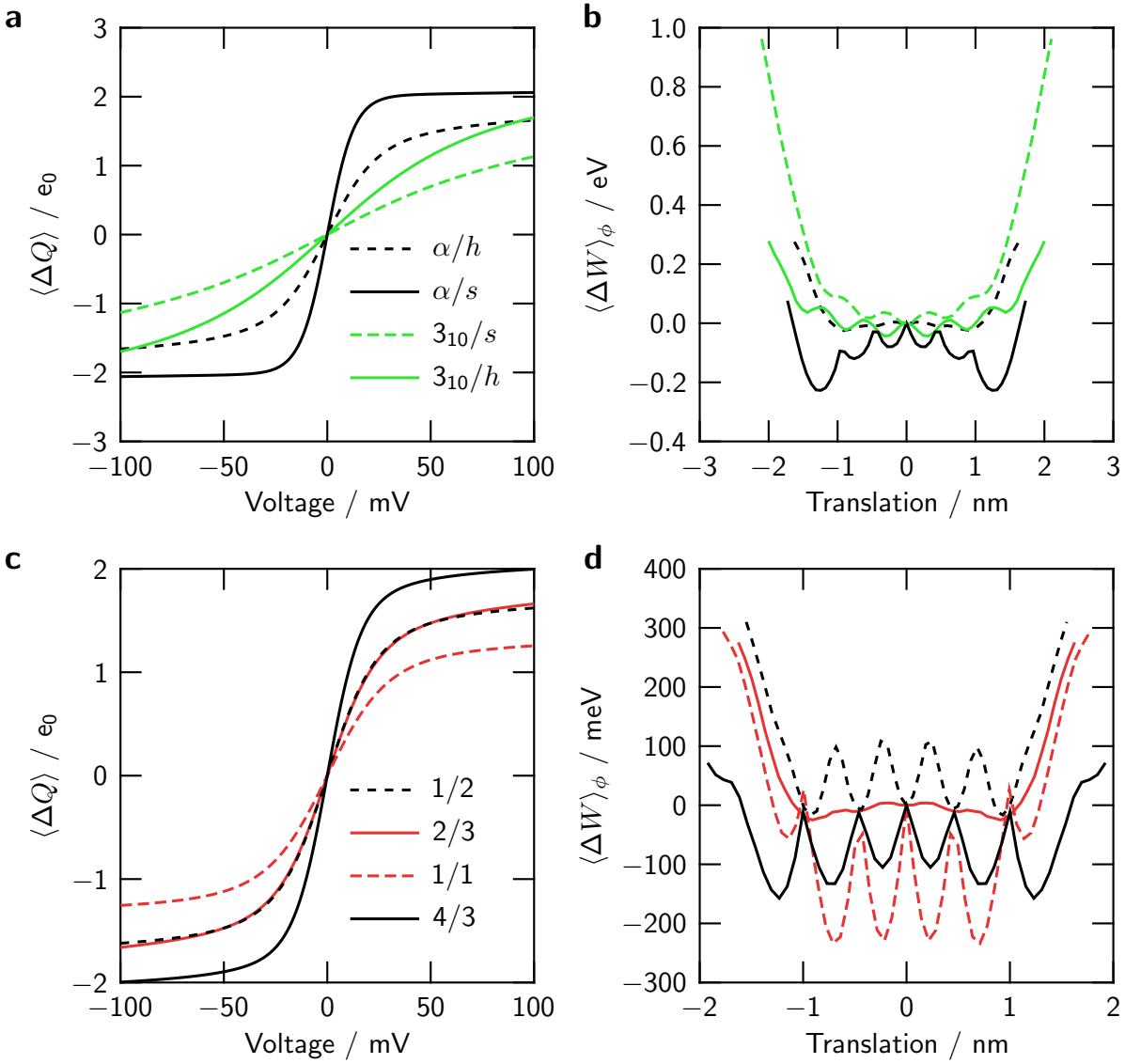

Peyser and Nonner (2012a, Fig. 4)

Dielectric coefficient

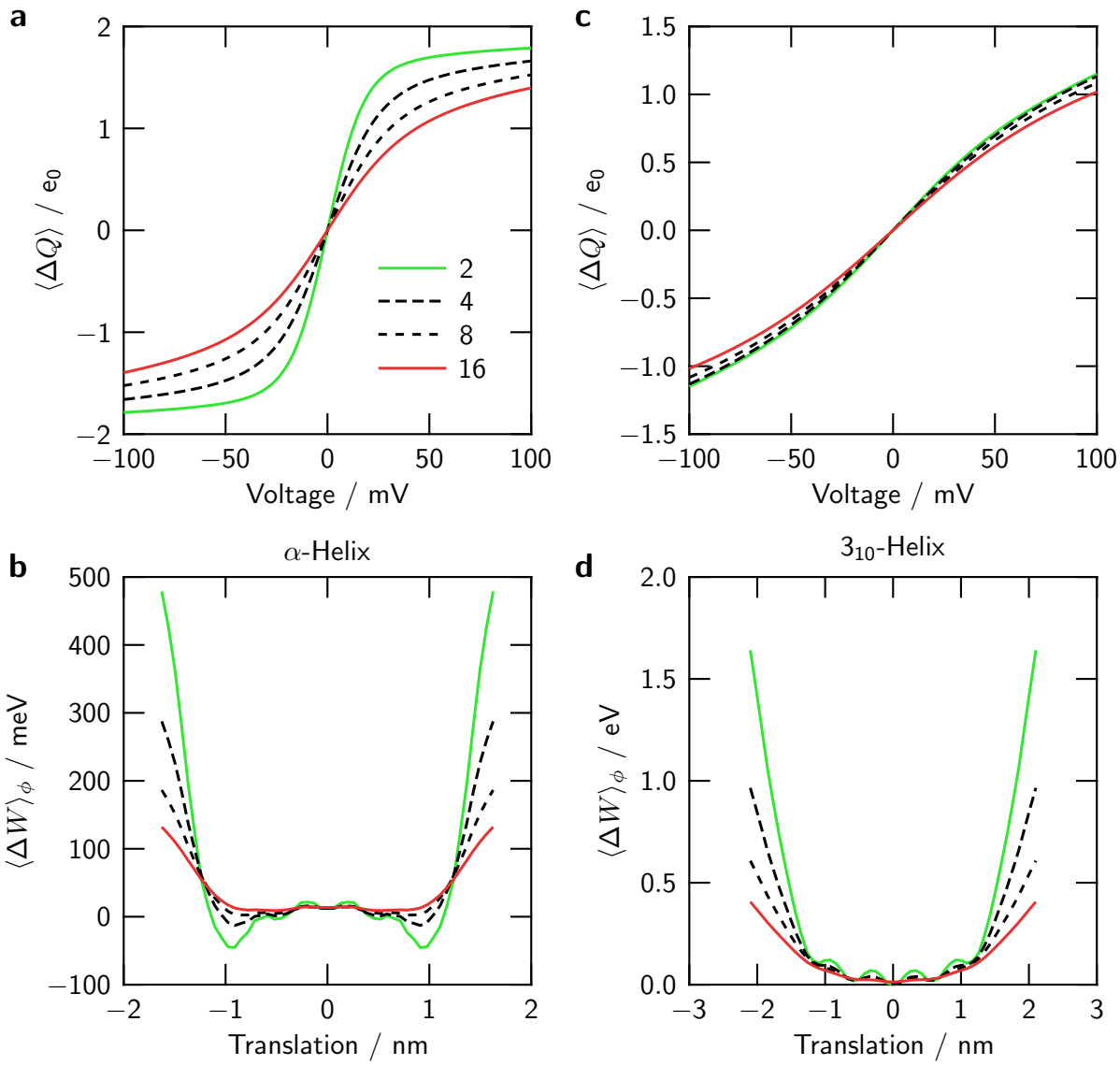

Peyser and Nonner (2012a, Fig. 5)

Gating canal geometry

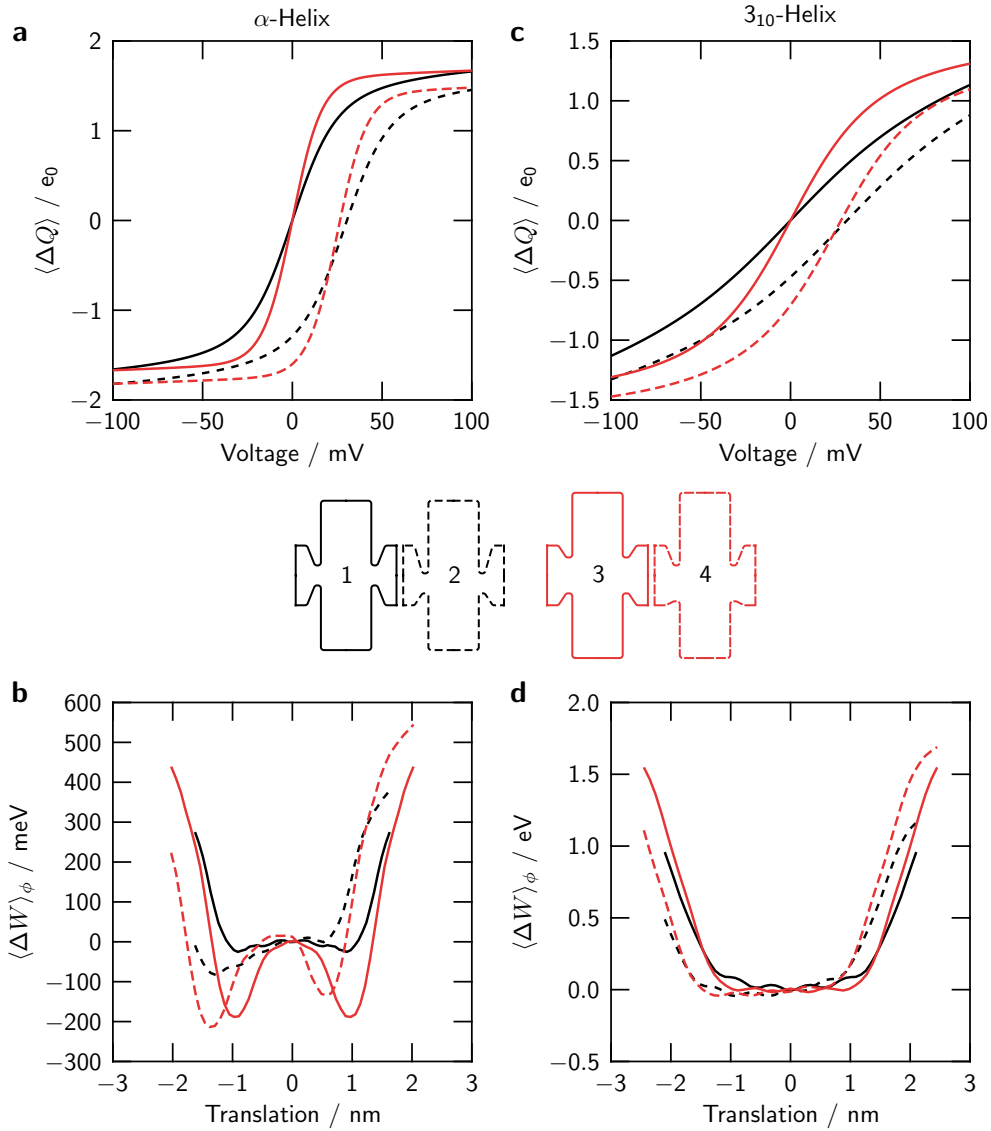

Peyser and Nonner (2012a, Fig. 6)

Bath screening

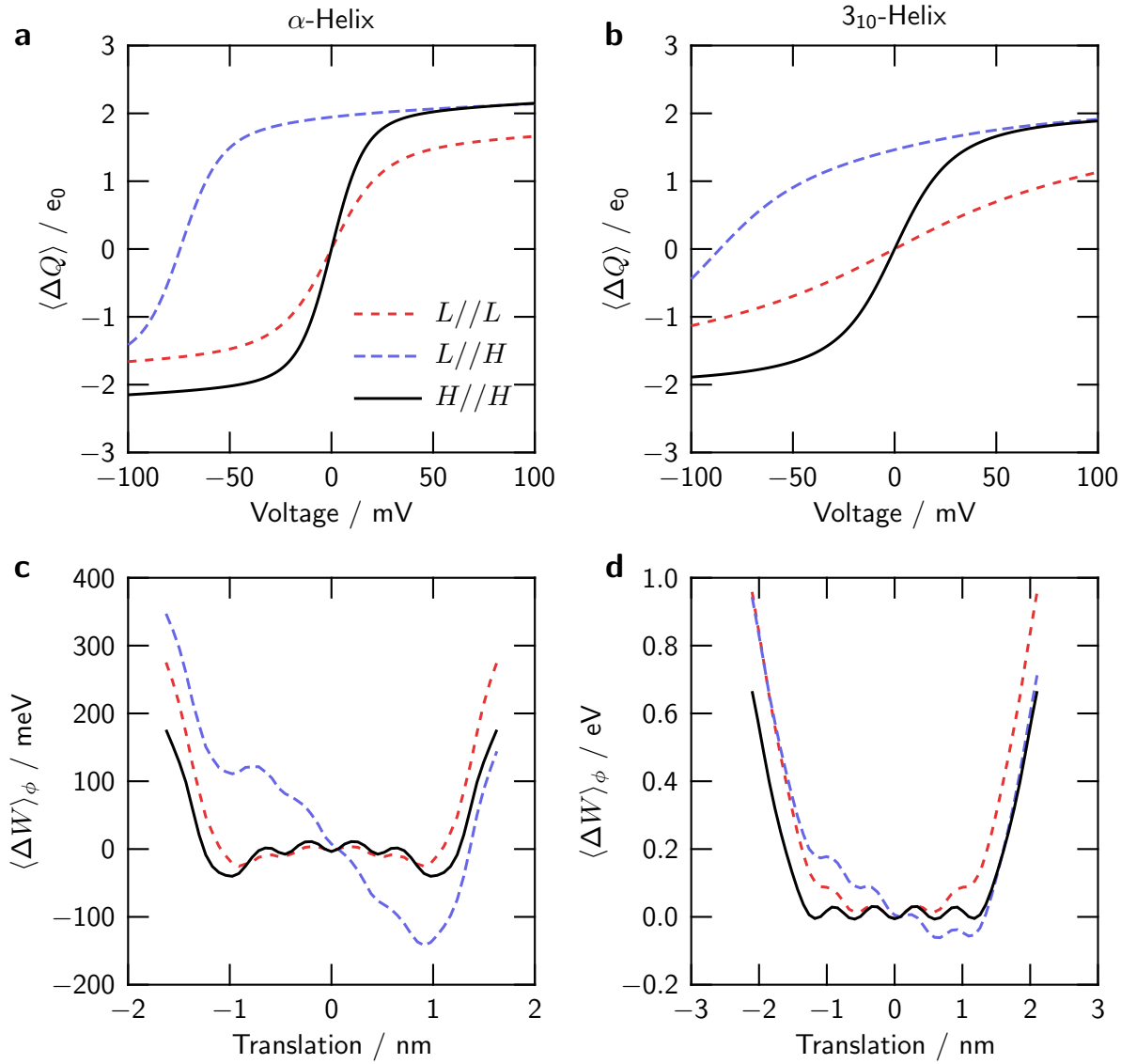

Peyser and Nonner (2012a, Fig. 7)

Surface charge

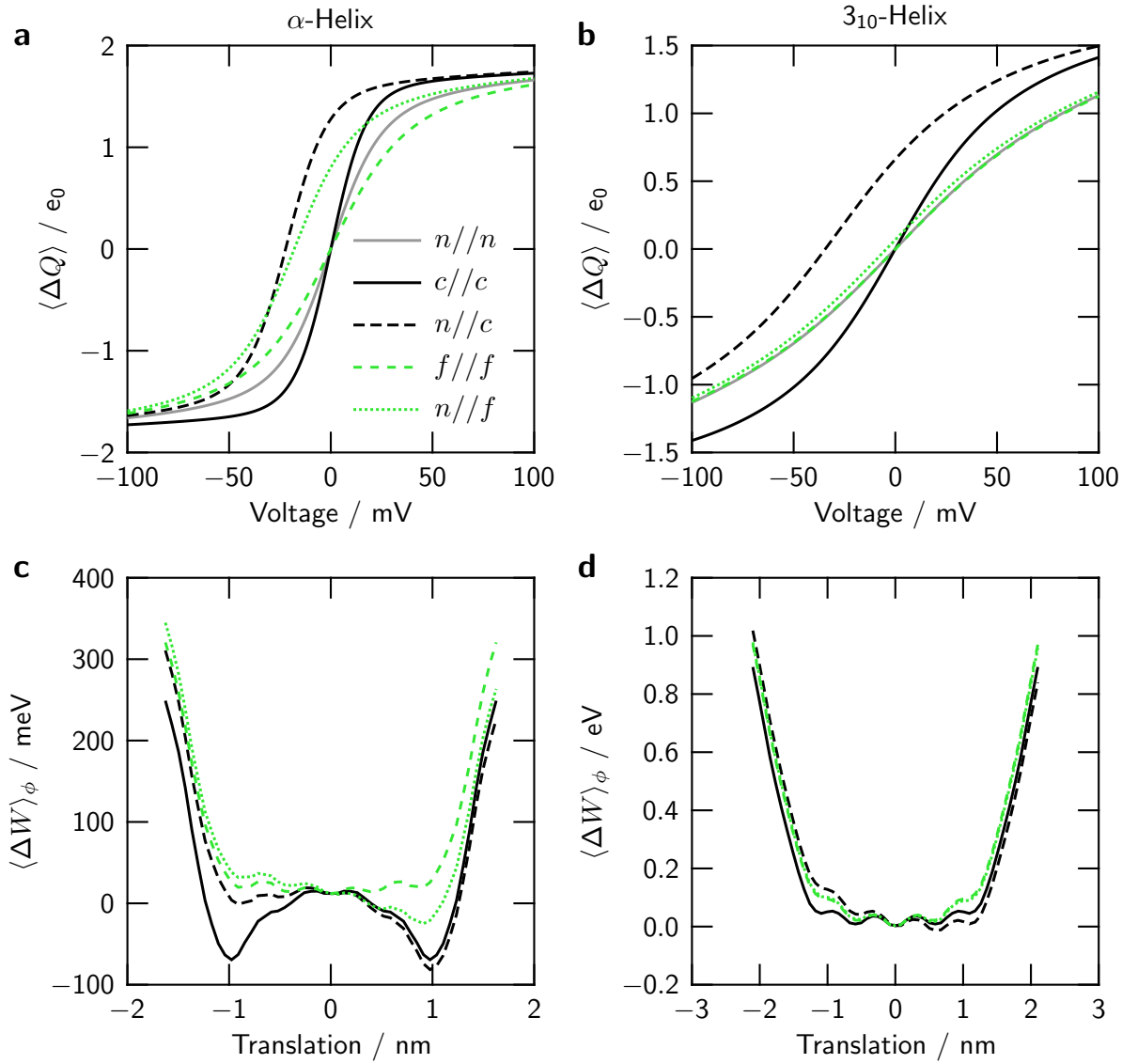

Peyser and Nonner (2012a, Fig. 8)

Load

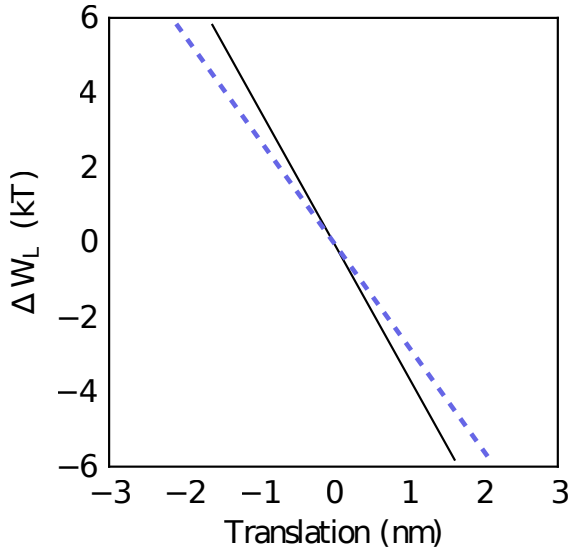

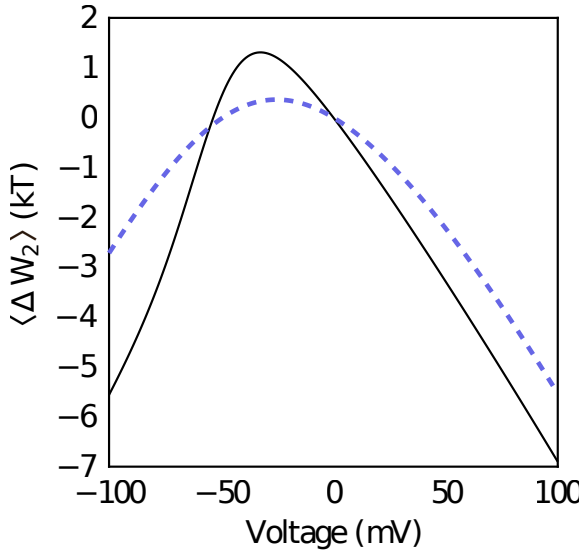

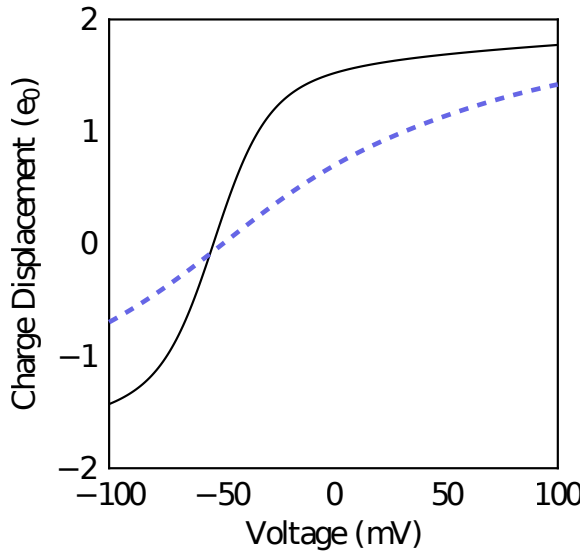

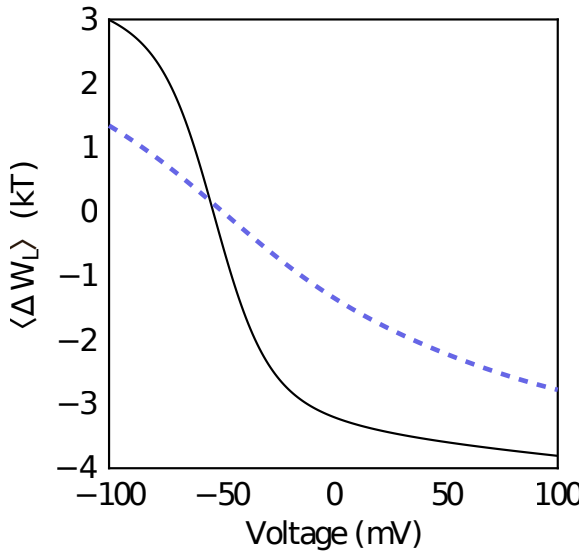

Peyser and Nonner (2012a, Fig. 8)

Multiscale gating

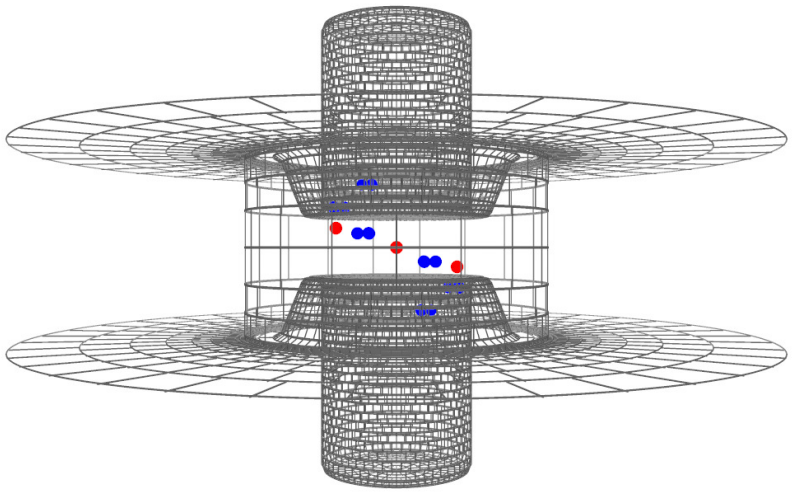

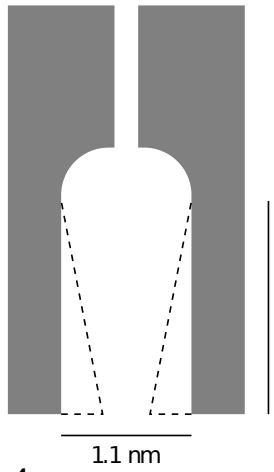

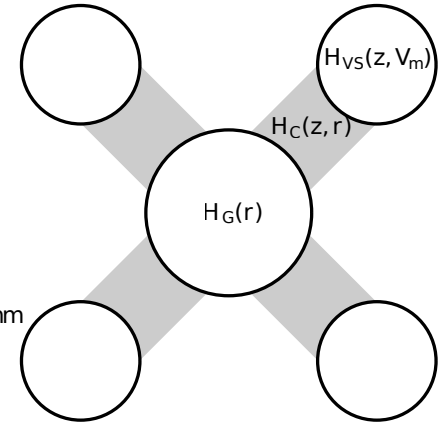

$$B(\mathbf{z}, r, V_\mathrm{m}) = \exp\{-\beta[\mathcal{H}_\mathrm{G}(r) + \sum_{i=1}^{4}(\mathcal{H}_{\mathrm{C},i}(z_i, r) + \mathcal{H}_{\mathrm{B},i}(z_i) + \mathcal{H}_{\mathrm{VS},i}(z_i, V_\mathrm{m}))]\}$$

$$\mathcal{H}_{\mathrm{VS},i}(z_i, V_\mathrm{m}) = -\beta^{-1} \ln \sum_j \exp\left[-\beta \mathcal{H}_{\mathrm{VS},i}(z_i, \phi_j, V_\mathrm{m})\right]$$

Hamiltonians & lower scale inputs

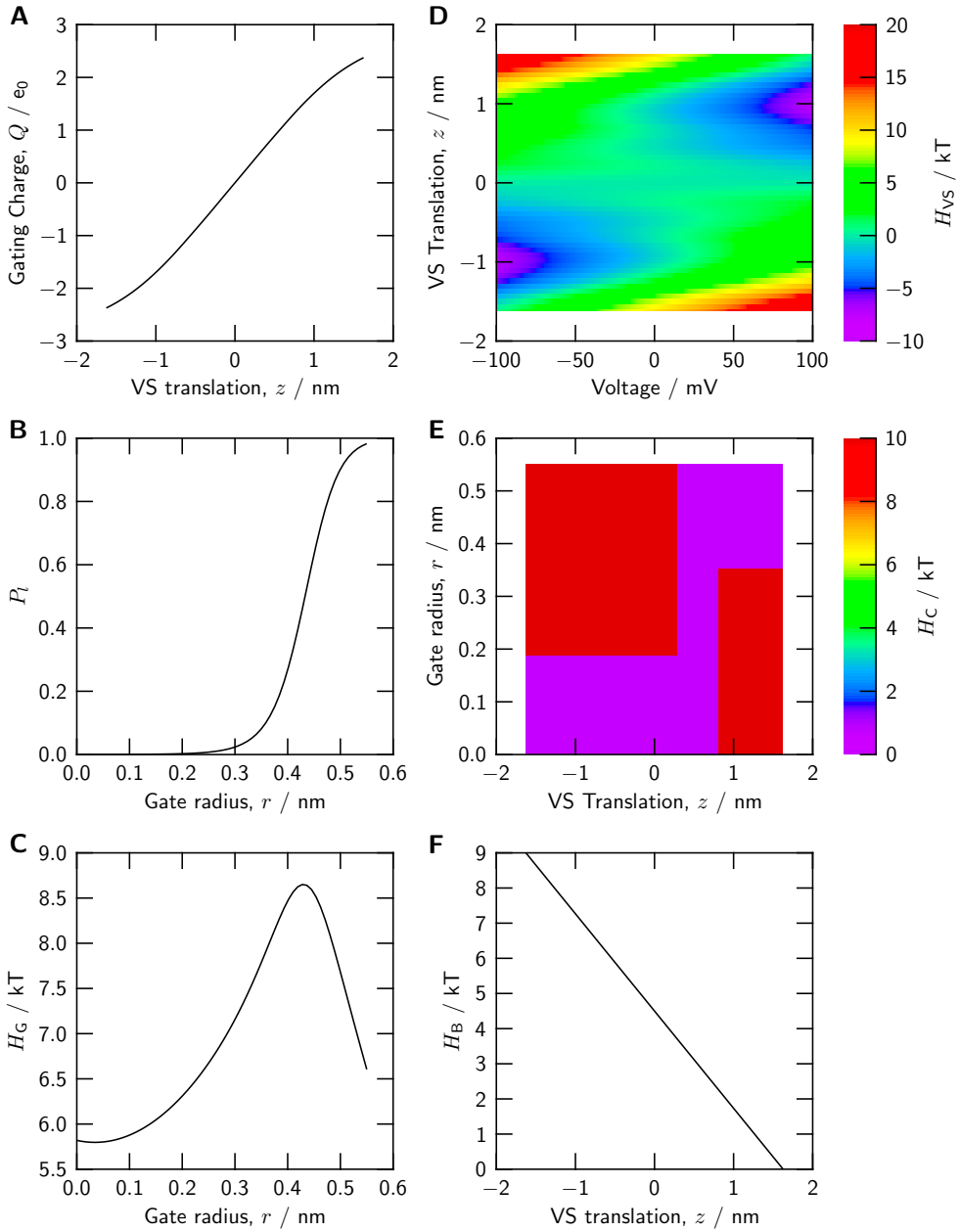

Full-channel experimental predictions

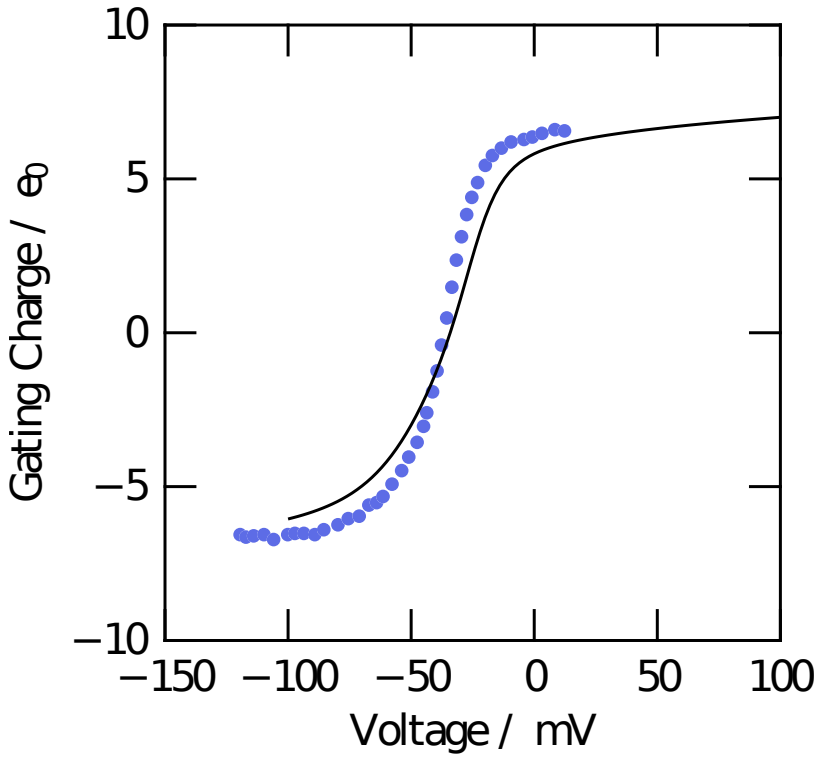

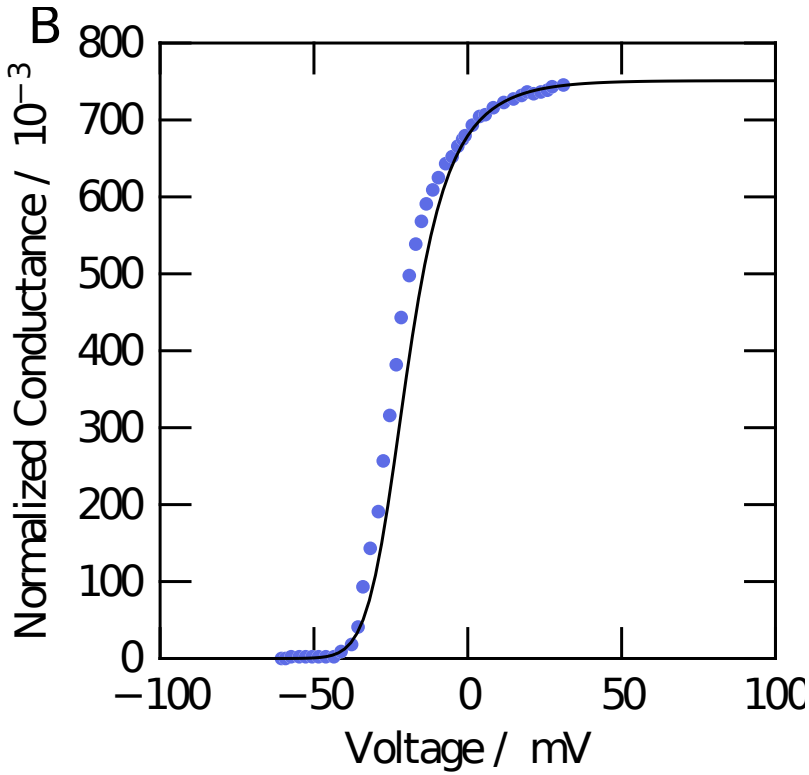

$$\mathcal{Q}(V_{\mathrm{m}}) = \sum_{l=1}^{N_r} \sum_{k_1=1}^{N_z} \sum_{k_2=k_1}^{N_z} \sum_{k_3=k_2}^{N_z} \sum_{k_4=k_3}^{N_z} n(k_1, k_2, k_3, k_4) B(z_{k_1}, z_{k_2}, z_{k_3}, z_{k_4}, r_l, V_{\mathrm{m}})$$

Acknowledgments

HPC in Neuroscience

Boris Orth
Andrew Adinetz
Martin Stöckle
Bastian Tweddell
Anne Do Lam-Ruschewski

German Research School for Simulation Sciences

Justin Finnerty

SimLab Neuroscience

Abigail Morrison
Rajalekshmi Deepu
Mikaël Naveau
Yury Zaytsev
Wolfram Schenck
Anna Lührs
Sven Strohmer
Susanne Kunkel
Markus Butz-Ostendorf

University of Miami

Wolfgang Nonner
Karl Magleby
Alice Holohean

Rush University

Bob Eisenberg
Dirk Gillespie

Universität Tübingen

Roland Roth

Funding

Deutsche Forschungsgemeinschaft
Helmholtz Association:
SMBH: Supercomputing and Modelling for Human Brain
JARA: Jülich Aachen Research Alliance
University of Miami
National Institutes of Health
NSF Graduate Research Fellowship
German Research School for Simulation Sciences

Any opinions, findings, conclusions or recommendations expressed in this publication are those of the author and do not necessarily reflect the views of any funders.

References I

C. Armstrong and F. Bezanilla. Currents related to movement of the gating particles of the sodium channels. Nature, 242(5398):459–461, 13 Apr. 1973. doi: 10.1038/242459a0.

C. S. Gandhi and E. Y. Isacoff. Molecular models of voltage sensing. J Gen Physiol, 120:455–463, Oct. 2002. doi: 10.1085/jgp.20028678.

Z. He. Review of the Shockley-Ramo theorem and its application in semiconductor gamma-ray detectors. Nuclear Instruments and Methods in Physics Research Section A: Accelerators, Spectrometers, Detectors and Associated Equipment, 463(1–2):250–267, 2001. ISSN 0168-9002. doi: 10.1016/S0168-9002(01)00223-6.

A. Hodgkin and A. Huxley. A quantitative description of membrane current and its application to conduction and excitation in nerve. J Physiol, 117(4):500–544, 1952. ISSN 00223751. URL http://www.ncbi.nlm.nih.gov/pmc/articles/PMC1392413.

References II

M. O. Jensen, V. Jogini, D. W. Borhani, A. E. Leffler, R. O. Dror, and D. E. Shaw. Mechanism of voltage gating in potassium channels. Science, 336(6078):229–233, 2012. doi: 10.1126/science.1216533.

W. Nonner, A. Peyser, D. Gillespie, and B. Eisenberg. Relating microscopic charge movement to macroscopic currents: The Ramo-Shockley theorem applied to ion channels. Biophys J, 87(6): 3716–3722, 2004. ISSN 0006-3495. doi: http://dx.doi.org/10.1529/biophysj.104.047548.

A. Peyser and W. Nonner. Voltage sensing in ion channels: Mesoscale simulations of biological devices. Phys Rev E Stat Nonlin Soft Matter Phys, 86:011910, July 2012a. doi: 10.1103/PhysRevE.86.011910.

A. Peyser and W. Nonner. The sliding-helix voltage sensor: mesoscale views of a robust structure-function relationship. Eur Biophys J, 41: 705–721, 2012b. ISSN 0175-7571. doi: 10.1007/s00249-012-0847-z.

References III

S.-A. Seoh, D. Sigg, D. M. Papazian, and F. Bezanilla. Voltage-sensing residues in the S2 and S4 segments of the Shaker K^+ channel. Neuron, 16(6):1159–1167, 1 June 1996. ISSN 0896-6273. doi: 10.1016/S0896-6273(00)80142-7.

X. Tao and R. MacKinnon. Functional analysis of Kv1.2 and paddle chimera Kv channels in planar lipid bilayers. J Mol Biol, 382(1):24–33, Sept. 2008. doi: 10.1016/j.jmb.2008.06.085.